UNIVERSITÉ DE LORRAINE

DENSYS
MASTER ERASMUS MUNDUS | DECENTRALISED SMART ENERGY SYSTEMS

Case-based module:

Optimizing hydrogen outlet pressure & current density & membrane thickness for a PEM electrolyzer

Amin Rooberahan
Keith Kudakwashe Gumbo
Kira Zhmud
Rajnesh Kumar
Sara-Medina Šehović

Supervisor:
Gael Maranzana

Nancy, February 2024

Table of Contents

1. Introduction

Green hydrogen, produced through water electrolysis using renewable electricity, is anticipated to play a pivotal role in the future energy landscape. Beyond substituting fossil hydrogen as a feedstock in established industries like ammonia and fertilizer production, which currently account for approximately 50% of global hydrogen production [1], green hydrogen is poised to assume a central position as an energy carrier in burgeoning markets such as the mobility sector and the renewable energies [2, 3]. Additionally, green hydrogen holds the potential to serve as feedstock for e-fuel production and act as a reducing agent in the steel industry [4-8]. Currently, only about 1–2% of the annual consumption of 70 million tonnes of hydrogen is produced using renewables [1]; however, to achieve the ambitious European emission targets, a substantial portion of both established and emerging markets must transition to being served by water electrolysis and renewable electricity in the future.

Efficient storage and transportation of hydrogen require the reduction of volume through either pressurization or liquefaction. Conventionally, hydrogen pressurization to the necessary end-use pressure involves the use of a mechanical compressor. Hydrogen, being a very light and voluminous gas, demands a substantial amount of energy for compression, as illustrated by the green curve in Fig. 1. The isothermal compression work required to move from 0.1 to 100MPa constitutes over 7%of the hydrogen energy content (specifically, 7.2%of LHV_{H_2}, which is the low heating value of hydrogen at 120MJ/kg). It's crucial to note that this calculation only accounts for the mechanical energy transferred in an ideal isothermal compression scenario, and additional losses must be considered. Any increase in hydrogen temperature during compression, friction within the compressor, or inefficiencies in the electric motor will further elevate the energy expended. Furthermore, one must consider the factor in the efficiency of converting chemical energy into electric energy production (around 50% in optimal scenarios). Consequently, without careful handling, the compression process could result in a loss exceeding 20% [9].

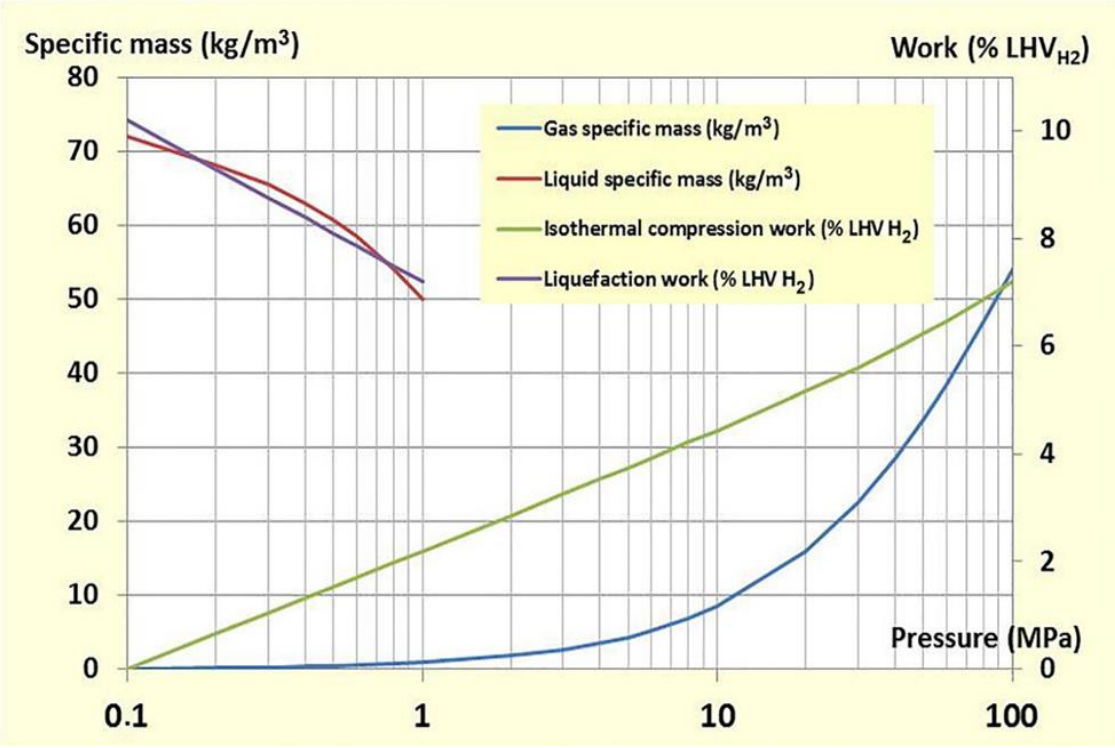

Figure 1. Specific mass and minimum work for compression and liquefaction of hydrogen as a function of pressure, as in [9].

However, considering equipment count, process complexity, and plant reliability, an appealing alternative is the internal pressurization of the gas within the electrolyzer [10]. Electrolytic devices, employing electrical energy to separate water into hydrogen and oxygen, stand as a crucial technology in generating environmentally friendly hydrogen from renewable or nuclear power. The capacity for electrolysis dedicated to hydrogen production has witnessed notable expansion in recent years [11]. Proton exchange membrane water electrolysis (PEMEL) is compatible with high-pressure performance. Presently, commercial PEMEL systems operate at hydrogen outlet pressures of 30–40 bar. However, prototypes capable of delivering hydrogen at several hundred bars have been successfully proven possible [12, 13, 14]. This capability is facilitated by the solid polymer electrolyte, which can withstand substantial pressure gradients across the cells. This stands in contrast to alkaline water electrolyzer systems, which are restricted to balanced pressure operation due to the utilization of porous separators [15]. In differential pressure PEMELs, pressurization is achieved electrochemically, eliminating the need for a water pressurization pump or high-pressure components in the balance-of-plant on the oxygen side. Additionally, the handling of compressed oxygen gas is not required. Consequently, these systems are inherently safer, less complex, and produce higher-purity gas compared to balanced-pressure electrolyzers [16].

Operating PEM electrolyzers at pressure levels suitable for relevant end-use applications offers various benefits. Notably, it becomes feasible to remove the mechanical compressor from the system. This substitution replaces a large, expensive, and loud component that is susceptible to breakdowns and necessitates frequent maintenance. In addition to the benefits of reduced system capital expenditure (CAPEX) and complexity, elevating the electrolyzer pressure opens up the potential to increase the plant's capacity or decrease the size of system components by a factor equal to the pressure ratio. The allure of these potential advantages in high-pressure PEM electrolysis has garnered interest in both academic and industrial circles. This interest has served as the driving force behind research activities, including those at IFE, leading to the establishment of a flexible PEMEL system laboratory designed for testing stacks with hydrogen outlet pressures up to 200 bar [17].

A significant weakness of high-pressure differential operation in PEMELs is the relatively elevated hydrogen diffusion through the membrane from the hydrogen side to the oxygen side. This leads to a reduction in the amount of usable hydrogen and, consequently, a decrease in the faradaic efficiency of the system. The concentration of hydrogen in oxygen may even surpass the lower flammability limit (LFL) of 4 vol%, requiring the inclusion of anodic gas recombination catalysts. Another drawback is the delicate mechanical strength requirements, as the anode cell components bear all the pressure from the cathode side. To address this, it may be necessary to employ thick or reinforced membranes, porous transport layers, and limitations on the active area. However, these adjustments result in increased ohmic losses and could present challenges in terms of scaling up the system [16].

Fig. 2 illustrates examples of current and prospective applications for green hydrogen, along with their associated pressure levels [16]. Low-pressure applications, which can be accommodated by existing electrolyzer technologies without the need for a mechanical compressor, encompass metal hydride storage (10–40 bar) [18, 19, 20] and metallurgical processes like steel production (5–10 bar) [4, 5, 51, 52]. Metal hydride storage (10–40 bar) is appealing for onboard storage, especially in applications like trains where safety requirements are stringent, and weight limitations are comparatively relaxed compared to other transport applications. Intermediate pressure applications, such as e-fuel and e-methanol production, which require a hydrogen stream of up to 100 bar, can benefit from elevated electrolyzer operating pressures [7, 8, 21]. Another intermediate pressure use case with significant potential is the injection of hydrogen into the natural gas grid (at approximately 70 bar) [22]. Leveraging the existing gas grid infrastructure facilitates the rapid transportation of substantial hydrogen volumes from the generation source to the market. This application has the potential to expedite the transition for very large volume users. Within the realm of medium-to-high-pressure

applications, various instances showcase the diverse pressure requirements. Ammonia production operates within the range of 200–300 bar [23], while gaseous storage finds its place in salt caverns at pressures ranging from 130 to 200 bar [24, 25]. Transport cylinders offer flexibility in pressure, with values spanning from 180 to 500 bar [26]. Each of these applications demonstrates the versatility of medium-to-high-pressure utilization. Moving to the transportation sector, heavy-duty vehicles, including buses, trucks, and ferries, rely on onboard tanks functioning at a pressure of approximately 350 bar. As the pressure spectrum increases, passenger cars stand out with onboard tanks requiring pressures as high as 700 bar. Moreover, to facilitate efficient gas transfer, hydrogen refueling pressures for passenger cars can escalate to demanding levels of up to 950 bar [10, 27]. It is in this high-pressure domain of passenger car applications that the replacement of the mechanical compressor becomes an exceptionally intricate and demanding task.

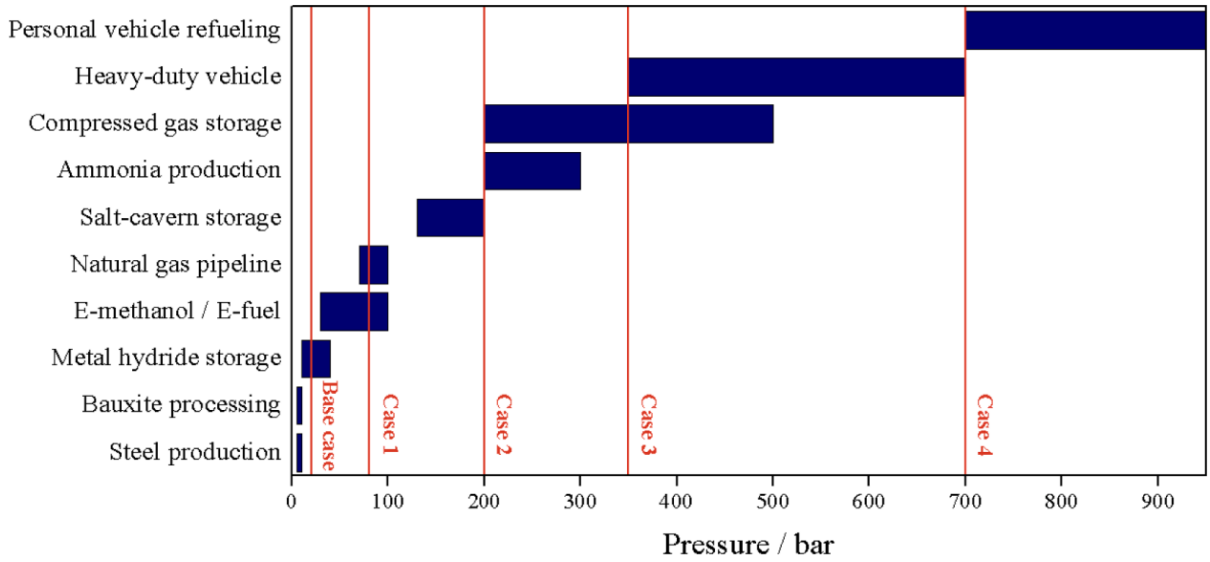

Figure 2. Existing and future applications for green hydrogen and corresponding pressure levels. The "base case" (30 bar) and the four investigated use cases (80 bar, 200 bar, 350 bar, and 700 bar) are indicated [16].

The main objective of this research is to optimize the electrochemical compression with a primary focus on producing high-pressure hydrogen to minimize the overall cost of hydrogen production. This optimization centers around the critical parameter of the intermediate pressure, specifically the pressure at the outlet of the electrolyzer to quantities higher than what has been done in the literature. The aim is to determine the highest pressure at which hydrogen can be produced efficiently, thereby reducing the need for subsequent compression stages. In the study presented in this research, a numerical study was conducted using MATLAB to implement and analyze the proposed model. The research specifically targeted the highest pressure for efficient hydrogen production based on the current density. By strategically optimizing the intermediate pressure, the research seeks to minimize the need for subsequent compression stages, thereby enhancing the cost-effectiveness and energy efficiency of the "electrolyzer-compressor" system. Creation of a comprehensive model for simulating the intricacies of hydrogen compression will be undertaken, considering factors such as compression ratio and energy consumption. Integration of the PEM electrolyzer and hydrogen compressor models into a unified system model will be conducted. This model aims to represent the evolution of the overall cost while also paying separate attention to the CAPEX and OPEX of both the electrolyzer and compressor at different intermediate pressures.

2. Review of electrolyzer technologies

Electrolyzer technology can be categorized into four types based on the operating environment, electrolyte, and diaphragm. These include Alkaline (ALK), proton exchange membrane (PEM), Solid oxide electrolysis cell (SOEC), and Anion exchange membrane (AEM) with the latter being the least employed.

2.1. Types of Electrolyzers

The alkaline water electrolysis, pioneered by Troostwijk and Diemann in 1789 stands out for its extended service life, absence of precious metal materials, and stacked components [28]. This technology, recognized as the first water electrolysis method, has gained widespread industrial use, establishing itself as the most mature and globally employed water electrolysis approach [29]. Operating at temperatures around 60–80°C, the alkaline electrolyzer employs an electrolyte typically consisting of a 20%–30% concentration of KOH or NaOH. During the electrolytic process, a reduction reaction takes place at the cathode, where water is reduced to 1 mol of hydrogen and 2 mol of OH^-. The resulting OH^- migrates from the cathode to the anode through a diaphragm. Simultaneously, an oxidation reaction occurs at the anode, transforming the hydroxyl ion OH^- into 0.5 mol of oxygen O_2 and 1 mol of water H_2O [30]. The detailed operational flow chart is illustrated in Fig. 3.

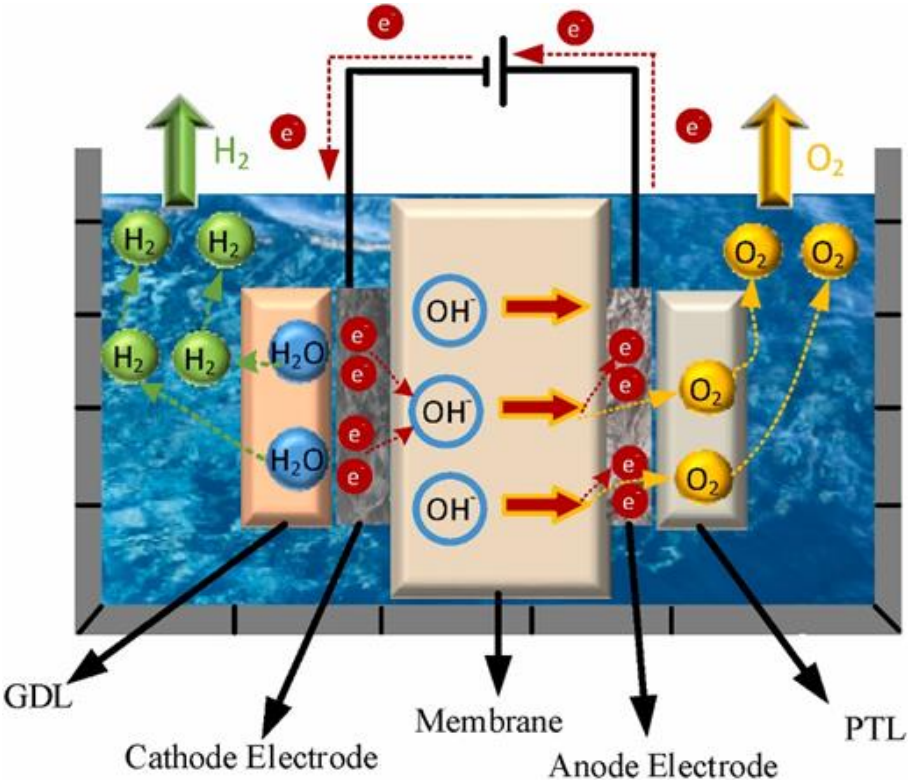

Figure 3. Alkaline electrolyzer working principle diagram [31].

In SOEC electrolytic water technology shown in Fig. 4 hydrogen production at high temperatures enhances thermodynamics and reaction kinetics, reducing the equilibrium voltage and power demand [32]. The use of cost-effective nickel electrodes contributes to lowered hydrogen production costs [33]. ALK, using concentrated KOH, offers inexpensive hydrogen production but faces efficiency challenges due to K_2CO_3 formation and asbestos mesh, reducing current and work efficiency. PEM electrolysis, employing precious metals like Pt and Ir in strongly acidic conditions, yields higher hydrogen production efficiency with a zero-spacing structure, reducing ohmic resistance

and outperforming ALK. AEM, resembling ALK, utilizes anion exchange membranes and transition metals, featuring a low-concentration alkaline solution for improved efficiency. SOEC stands out as the most efficient mainstream technology, leveraging excess heat for electrolysis and minimizing the reliance on electrical energy [32].

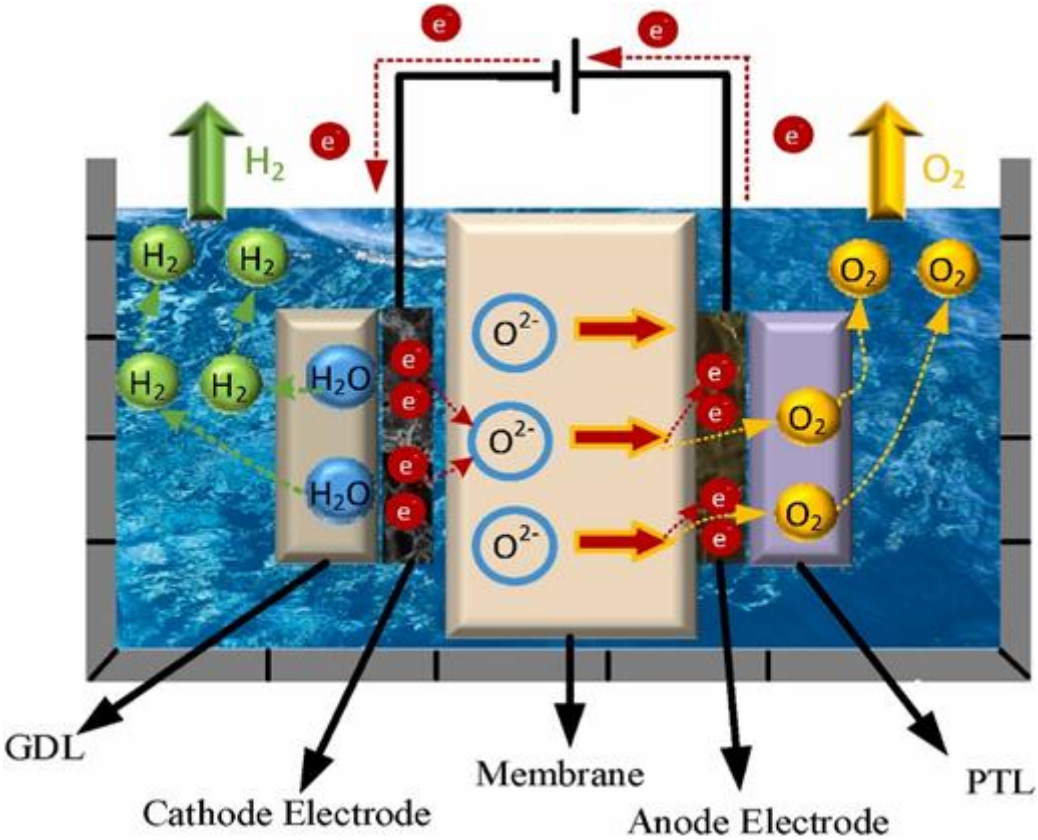

Figure 4. SOEC electrolyzer working principle diagram [31].

The PEM electrolytic water technology addresses the mixing issue of cathode and anode gases prevalent in alkaline electrolyzers using asbestos mesh as a diaphragm. Grubbs introduced PEM electrolysis as a solution, replacing the asbestos mesh with a proton exchange membrane (PEM) [34]. This membrane not only conducts protons but also isolates cathode and anode gases, offering higher current density and efficiency compared to ALK. The PEM technology enhances both hydrogen production rate and purity [35]. Operating at 50–80 ℃ with a current density of 1 A/cm^2 [34], PEM electrolyzers feature a zero-gap structure, reducing the electrolyzer's volume. During electrolysis, the anode side decomposes 1 mol of water into proton H+, electron e−, and oxygen O2. Protons and electrons travel through the PEM to the cathode side, where they recombine to produce hydrogen [30]. The basic working principle is illustrated in Fig. 4.

The Nafion membrane, a perfluorosulfonic acid polymer manufactured by Dupont, is widely adopted as a proton exchange membrane (PEM) in electrolyzers due to its commendable chemical stability, mechanical strength, thermal stability, and proton conductivity [36]. Liquid water introduction at the anode initiates dissociation into molecular Oxygen, Hydrogen Protons and electrons. Subsequently, the solvated protons migrate through the Nafion membrane to the cathode, where they undergo reduction to form molecular hydrogen.

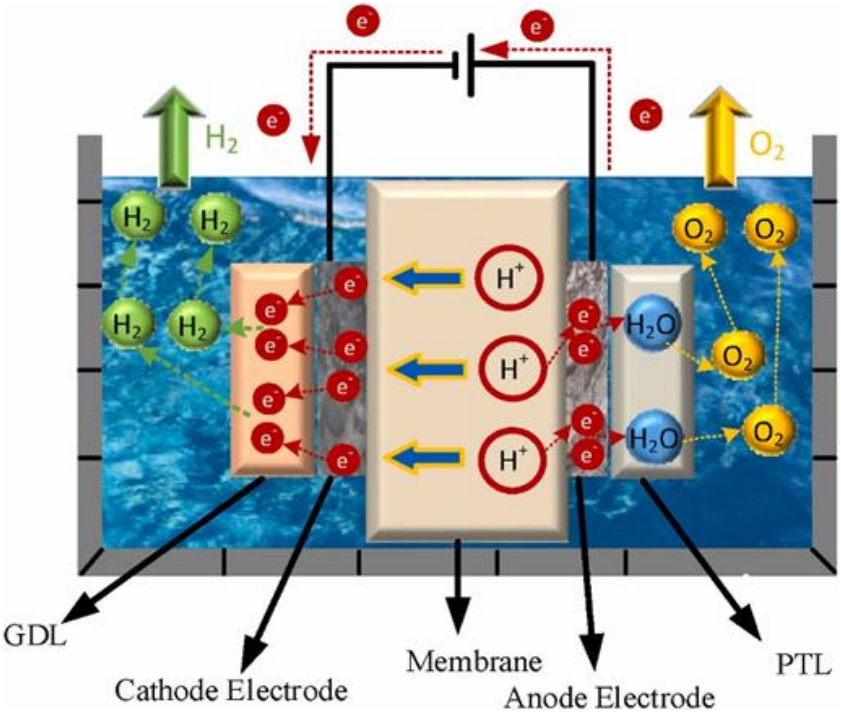

Figure 5. PEM electrolyzer working principle diagram [31].

Throughout this migration, water molecules accompany the protons through the membrane, facilitated by an electric field from the anode to the cathode. These reactions at the anode and cathode are shown below:

$$H_2O = H^+ + \tfrac{1}{2}O_2 + 2e \qquad \text{at the anode} \qquad \text{(A)}$$

$$2H^+ + 2e = H_2 \qquad \text{at the cathode} \qquad \text{(B)}$$

By employing membrane technology, the electrolyzer adopts pure water as the circulating fluid. This choice results in a more straightforward balance of plant and a reduction in leak current. Moreover, the gaseous products of hydrogen (H2) and oxygen (O2) are produced at the backside of the interpolar field, leading to lower ohmic loss and higher gas purity, as emphasized in references [12, 13].

Advancements in electrolyzer technology are evident on a global scale, with noteworthy contributions from key regions. China, positioned as a frontrunner in both installed and under-construction electrolyzer capacity, dominates global electrolyzer manufacturing, representing 40% of the current global capacity. The European Union demonstrates significant growth, installing around 80 MW of electrolyzer capacity in 2022, and the United States unveils crucial incentives through the Inflation Reduction Act (IRA), impacting electrolyzer manufacturing projects across the country [11].

Global electrolyzer manufacturing capacity surged to nearly 11 GW per year in 2022, marking a remarkable increase of over 25% compared to the preceding year. Europe and China jointly constitute two-thirds of the world's manufacturing capacity. Manufacturers are proactively expanding their production capacity, aiming to exceed 130 GW per year by 2030. Despite ambitious plans, less than 10% of the announced capacities for 2030 have reached a final investment decision (FID), underscoring uncertainty in future manufacturing capacity deployment [11]. This global surge in manufacturing capacity aligns with the widespread adoption of PEM electrolyzers and the utilization of Nafion membranes, reflecting the pivotal role played by these technologies in the evolving landscape of sustainable hydrogen production. A comprehensive overview of the properties of Nafion membranes, covering water uptake, swelling ratio, proton conductivity, and the electro-osmotic drag coefficient when exposed to and equilibrated with liquid water is done in this section.

2. 2. Water Uptake and Swelling

A critical aspect of Nafion membrane behaviour is its water uptake which can either be expressed through weight percent (ω) or water content (λ). The membrane's pre-treatment plays a pivotal role, impacting water uptake significantly. It is observed differences in water uptake (λ) between membranes dried at room temperature and those dried at an elevated temperature of 105 ℃ [37]. The dissimilarities in (λ) between these forms are attributed to the disintegration of ionic clusters in the polymer membrane during drying at elevated temperatures, near the glass transition temperature.

2. 3. Proton Conductivity

A pivotal property of Nafion membranes is proton conductivity (k), which depends on water content and temperature. Conducted experiments on a Nafion 117 membrane revealed that (k) increases linearly with water content (λ) at 30°C when $2 < (\lambda) < 22$ [37]. The temperature dependence of (k) was also measured in the range of 25 to 90 ℃ with a constant (λ) of 22. Springer et al. [63] correlated proton conductivity using an expression involving (λ) and the membrane temperature (T). Kopitzke et al. [54] presented another correlation for the protonic conductivity (k), taking into account the activation energy (E_k) and a constant (k_0). The data reported by various authors were compared, emphasizing the importance of these correlations in understanding and predicting proton conductivity.

2. 4. Electro-osmotic Drag Coefficient

As protons traverse through a PEM, they drag water molecules along in a phenomenon known as electro-osmosis. The electro-osmotic drag coefficient (n_{drag}) quantifies the number of water molecules "dragged along" per proton (H^+). Similar to proton conductivity, n_{drag} depends on the water content in the membrane [37]. Under PEM electrolysis conditions, n_{drag} is solely dependent on membrane temperature [64]. Experiments on electro-osmotic drag showed that ng (number of water molecules per produced H_2 molecule) was influenced by current density, temperature, and cathode pressure [38].

2. 5. Hydrogen crossover

The hydrogen crossover through the membrane is a major concern from the safety, durability and efficiency viewpoints, in proton exchange membrane (PEM) electrolyzers. This hydrogen crossover rate increases by pressure, temperature, and current density [39]. Fig. 6 illustrates the configuration of a Proton Exchange Membrane (PEM) electrolyzer cell and depicts the directional flow of reactants and products. Hydrogen is produced at the cathode, while oxygen is generated at the anode. A minor fraction of hydrogen and oxygen permeates through the membrane to reach the opposite sides.

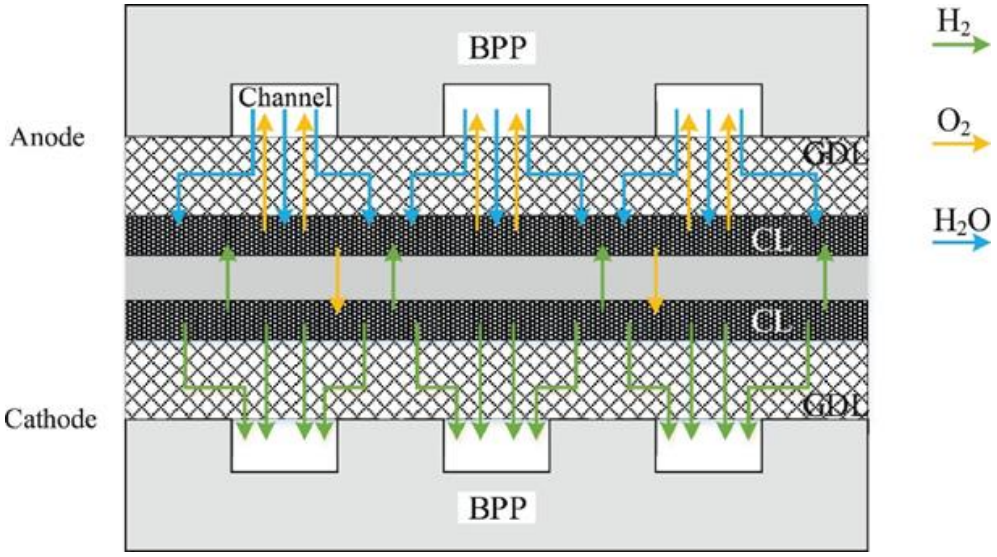

Figure 6. Schematic of a PEM electrolyzer: hydrogen and oxygen generation and gas crossover [39].

During Proton Exchange Membrane (PEM) electrolysis, 'i' represents the current density (in A cm^2). A portion of the hydrogen produced at the cathode side permeates through the membrane, mingling with oxygen on the anode side. The crossover of hydrogen through the membrane is intensified by elevating hydrogen pressure during electrolysis. It is crucial to maintain a safe hydrogen concentration on the oxygen side, aiming for levels below 2% to steer clear of the flammability limit set at 4%. The concentration of anodic hydrogen is influenced by factors such as membrane thickness (where a thicker membrane correlates with lower hydrogen crossover), cathodic hydrogen pressure, current density, and operating temperature [36, 40, 41]. At lower current densities, the anodic hydrogen concentration tends to be higher due to a reduced rate of oxygen generation (i.e., flow rate), resulting in an elevated hydrogen concentration.

Hydrogen concentration and crossover play crucial roles in water electrolysis. The process involves hydrogen super saturation before bubble nucleation, with the initiation of heterogeneous nucleation at the cathode catalyst layer (CL) surface remaining unclear [43]. Hydrogen super saturation increases until a critical level is reached, leading to bubble nucleation. This rise in saturation serves as the main driving force behind increased hydrogen crossover rates with current density [44, 45].

Hydrogen crossover through the membrane involves various factors such as the hydrogen diffusion coefficient, effective diffusion length, and hydrogen pressure on the membrane [40, 41]. Additionally, the diffusion coefficient in the membrane is estimated using parameters such as membrane water content, tortuosity factor, and hydrogen diffusion coefficient in water [42, 46]. The length of the diffusion path considers both the membrane thickness and the ionomer in the catalyst layer [47]. Hydrogen pressure on the membrane is affected by the current density, porous media characteristics, and pressure drop across the media [36, 40, 41].

In existing literature practices, the membrane thickness (t_m) is conventionally equated to (t_{diff}), and the hydrogen diffusion coefficient ($D_{H_2}^{eff}$) in the membrane is considered as ($D_{H_2}^{eff}$), yet this oversimplification may lead to an overestimation of the mass transfer coefficient at the cathode side. The assumption that ($t_{diff} = t_m$) when the membrane thickness approaches zero results in an inaccurate representation of the hydrogen crossover rate, as per the proposed model. It is argued that (t_m) should not be simply considered as the effective length of the diffusion path. Considering the increasing hydrogen concentration in the cathode catalyst layer, it becomes imperative to account for the thickness of the ionomer in both cathode and anode sides, which constitutes a significant proportion of the CL volume. The ionomer content in the cathode side, commonly around 30-35 w_t%, is estimated to be

approximately 15% of the CL volume, while on the anode side, it is around 20 w_t%, corresponding to roughly 11% volumetric ratio [48].

2. 6. Economical concerns of electrolyzers

CAPEX requirements for an installed electrolyzer system are currently in the range of USD 500 -1400/kWe for alkaline technology and USD 1100 - 1800/kWe for PEM, while estimates for SOEC range from USD 2800 - 5600/kWe [11]. The levelized cost of hydrogen production (LCOH) is a comprehensive analysis that takes into account both capital and operating costs associated with the hydrogen production process. It's important to note that the LCOH specifically addresses the costs involved in the production phase and does not incorporate expenses related to hydrogen storage and transportation.

The existing levelized cost for blue hydrogen production usually falls within the USD 2.8-3.5 per kg range, determined by gas prices ranging from USD 6-11 per MMBtu. The capital cost encompasses various components, including the reformer unit, steam turbine, essential balance of plant, and other units depending on the technology employed, such as SMR and ATR. Similar to green hydrogen, the operational cost of blue hydrogen incorporates expenses associated with numerous variable and fixed parameters [65].

The current levelized cost of producing green hydrogen ranges from USD 3 to 6 per kg, rendering it economically impractical. The cost is heavily dependent on factors such as the capital cost of electrolyzers (CAPEX), their capacity or utilization factor (OPEX), and the cost of procuring renewable electricity. CAPEX covers expenses associated with the electrolyzer system or stack, balance of plant components, and electricity grid connection, while OPEX includes costs related to various variable and fixed parameters. Currently, hydrogen production relies predominantly on fossil fuel technologies without emission controls. However, in the Net Zero Emissions by 2050 Scenario, the focal point shifts to low emission. The capacity for electrolysis is expanding from a minimal starting point and necessitates a substantial acceleration to align with the Net Zero Emissions by 2050 Scenario [11].

Critical for generating low-emission hydrogen from renewable or nuclear electricity, electrolyzers have seen growth in their capacity for dedicated hydrogen production in recent years. However, the momentum decelerated in 2022, witnessing only about 130 MW of new capacity coming online, marking a 45% decrease compared to the preceding year. On a positive note, electrolyzer manufacturing capacity has surged by over 25% since the previous year, reaching nearly 11 GW annually in 2022. If all the projects in the pipeline materialize, the installed electrolyzer capacity could range from 170 to 365 GW by 2030 [11].

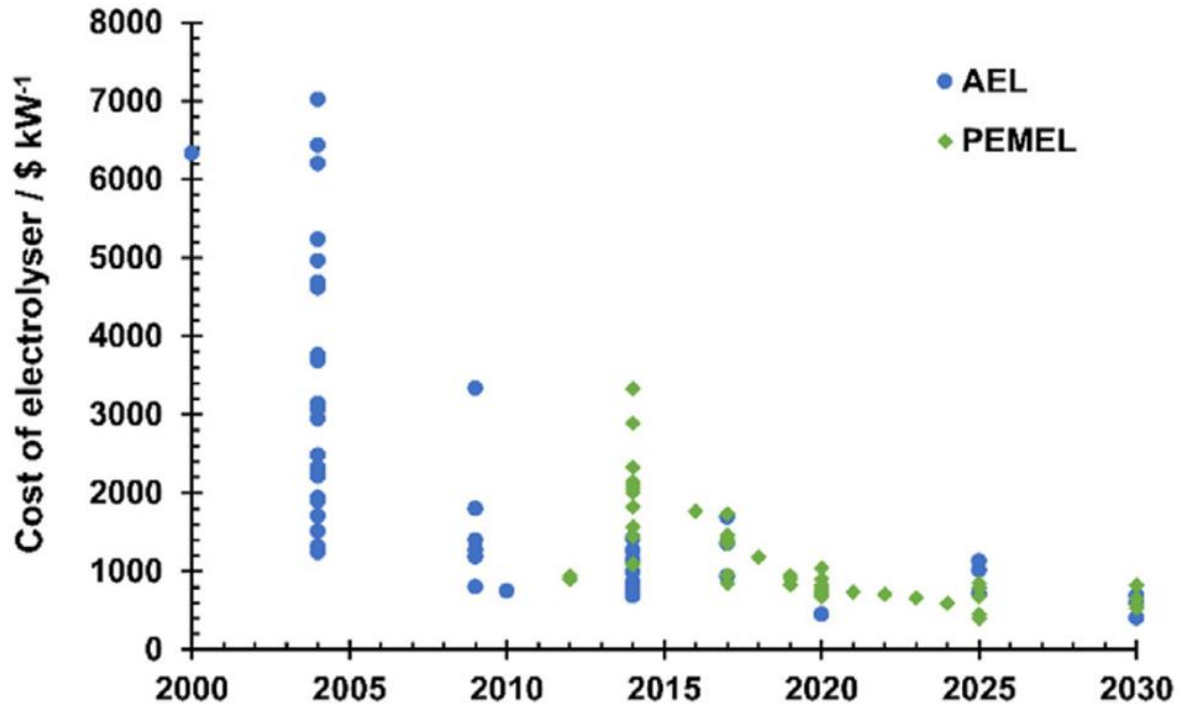

Figure 7. Literature data for electrolyzer costs from 2000 until [49].

2. 7. Advancement in Electrolyzer Technology

Electrolyzers have found extensive use in the chlor-alkaline industry for chlorine and sodium hydroxide production, amassing an installed capacity exceeding 20 GW. However, the dedicated deployment of electrolyzers for hydrogen production gained momentum only in the late 2010s. The year 2021 marked a record for deployment, with over 200 MW of electrolysis capacity becoming operational. However, in 2022, despite promising project announcements, capacity additions decelerated to 130 MW, resulting in a total installed capacity of approximately 690 MW [11].

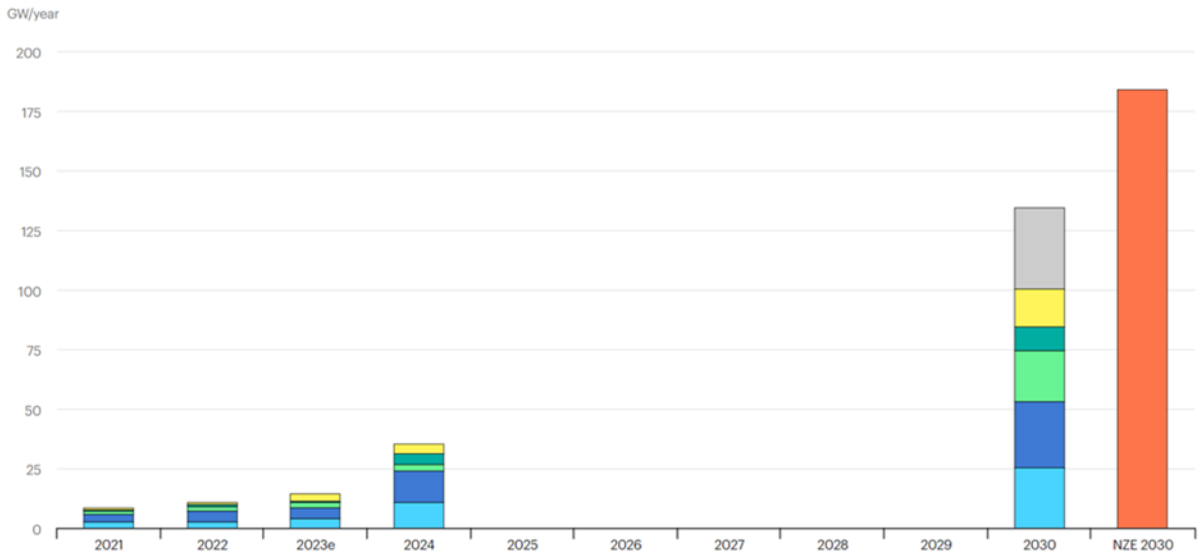

Figure 8. Announced electrolyzer manufacturing capacity by region and manufacturing capacity needed in the Net Zero Scenario, 2021-2030 [50]

Anticipating a surge in future demand, manufacturers have initiated the expansion of their production capacity. In 2022, global electrolyzer manufacturing capacity surged to nearly 11 GW per year, marking a remarkable increase of over 25% compared to the preceding year. Europe and China jointly constitute two-thirds of the world's manufacturing capacity. Despite capacity additions of electrolyzers for dedicated hydrogen production in the range of tens to hundreds of MW in recent years, the global manufacturing capacity for this technology remains largely underutilized, even when accounting for deployments related to chlor-alkali applications. Manufacturers are proactively expanding their production capacity, driven by the current market growth, an escalating number of large-scale project announcements, expectations of future demand growth, and the long-term nature of decisions associated with establishing substantial manufacturing facilities. According to company announcements, the global manufacturing capacity for electrolyzers has the potential to exceed 130 GW per year by 2030. This represents a one-third increase from the capacity in the pipeline at the end of 2022. The announced electrolyzer manufacturing capacity has the capacity to meet the targets outlined in existing national strategies, constituting almost three-quarters of the capacity needed in the Net Zero Emissions Scenario (NZE). Europe and China are projected to maintain their leadership, each contributing around a fifth of this expanded capacity. Despite these ambitious plans, it's noteworthy that less than 10% of the announced capacities for 2030 have reached a final investment decision (FID), and a quarter have been announced without specifying a location. This underscores a level of uncertainty regarding future manufacturing capacity deployment, an aspect that could be significantly influenced by each country's supportive policy framework [11].

3. Methodology

The compressed hydrogen production system is presented in Fig. 9 In this report, such a system is optimized to minimize the levelized cost of hydrogen (LCOH). The optimization parameters are the intermediate pressure P_{H2} after the PEM electrolyzer, the current density of the electrolyzer I_{el}, and the thickness of the membrane t_m.

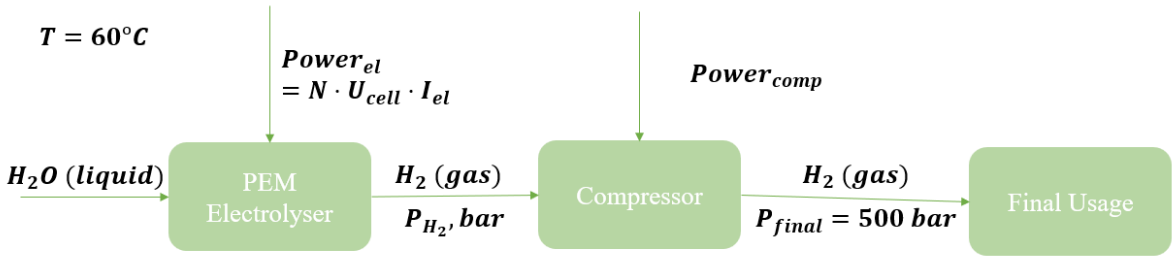

Figure 9. The system of compressed hydrogen production

The following section deals with the techno-economical model. The system is composed of a PEM electrolyzer whose number of cells is $N = 1$ and a mechanical compressor. The final usage of hydrogen is not covered by this techno-economical model.

3. 1. Electrolyzer model

Cell voltage U_{cell} is calculated as the sum of the Nernst potential U_N, ohmic overvoltage U_{ohm} and kinetic overvoltage U_{kin}.

$$U_{cell} = U_N + U_{ohm} + U_{kin} \tag{1}$$

The Nernst equation allows us to determine the potential of a cell in non-standard conditions. The Nernst potential U_N and is calculated using the formula [15]:

$$U_N = U_{rev} + \frac{R \cdot T}{2 \cdot F} ln\left(\frac{P_{H_2}^c \sqrt{P_{O_2}^a}}{{P_{ref}}^{3/2}}\right) \tag{2}$$

where $P_{ref} = P_0 = 1\ atm = 10^5\ Pa$, which denotes standard ambient pressure. U_{rev} is the reversible potential. The Nernst potential equation can be rewritten as

$$U_N = U_{rev}^{P_0} + \frac{R \cdot T}{2 \cdot F} ln\left(\frac{P_{H_2}^c \sqrt{P_{O_2}^a}}{{P_0}^{3/2}}\right) \tag{3}$$

where reversible potential U_{rev}, considering the pressure $P_0 = 1\ atm$, is calculated as a function of P_0 and T [53]:

$$\begin{aligned} U_{rev}(T,P) &= U_{rev}^{P_0}(T, 1\ atm) \\ &= 1.5184 - 0.0015421 \cdot T + 9.523 \cdot 10^{-5} \cdot T \cdot lnT + 9.84 \cdot 10^{-8} \cdot T^2 \end{aligned} \tag{4}$$

The ohmic overpotential is calculated as

$$U_{ohm} = (R_{el} + R_m) \cdot I = R_\Omega \cdot I \tag{5}$$

where contact resistances $R_{el} = 20 \cdot 10^{-7}\ [\Omega.\mathrm{m}^2]\ and\ R_m$ is the protonic resistance of the membrane, calculated below. The losses caused by the resistance to the flow of electric current through the cell component are dominated by contact resistances $\mathrm{R_{el}} = 20 \cdot 10^{-7}\ [\Omega.\mathrm{m}^2]$.

$$R_m = \frac{t_m}{\sigma_m} \tag{6}$$

where t_m is the thickness of the membrane and σ_m is the proton conductivity of the membrane [54]:

$$\sigma_m = \sigma_m^{H^+} = (0.519\lambda_m - 0.326)exp\left[1263\left(\frac{1}{303} - \frac{1}{T}\right)\right] \tag{7}$$

In this equation, the water content in membrane, denoted as λ_m, has a value of $\lambda_m = 20\frac{mol_{H_2O}}{mol_{SO_3}}$ [55].
The water content in membrane λ_m is a form to express the water uptake by a Nafion membrane. It represents the number of water molecules per sulfonic acid site [55].
Implementing formula (7) into formula (6), we deduce the final formula for R_m:

$$R_m = \frac{t_m}{(0.519\lambda_m - 0.326) \cdot exp\left[1263\left(\frac{1}{303} - \frac{1}{T}\right)\right]} \tag{8}$$

The kinetic overvoltage U_{kin} is the sum of the activation barrier on the anode and the cathode:

$$U_{kin} = b(T)ln\left(\frac{I_{el}}{I_0(T)}\right) \tag{9}$$

where the following coefficients are obtained from the experimental data:

$$b = 0.0227\ V$$

$$I_0 = 0.0062 \cdot 10^4 \frac{A}{m^2}$$

After calculation of the cell voltage U_{cell}, the power provided to the electrolyzer expressed in the unit of $\frac{W}{m^2}$ can be calculated using the formula:

$$Power_{el} = U_{cell} \cdot I_{el} \cdot N \tag{10}$$

where N denotes the number of cells.

To calculate the hydrogen permeation (diffusion at the anode), we use the following formula [15]:

$$\dot{n}_{H_2}^a = \frac{D_{H_2}^m H_{H_2} P_{H_2}^c}{RTt_m} \tag{11}$$

Similarly, we can calculate the oxygen permeation (diffusion at the cathode) through the membrane:

$$\dot{n}_{O_2}^c = \frac{D_{O_2}^m H_{O_2} P_{O_2}^a}{RTt_m} \tag{12}$$

ere $D_{H_2}^m$, $D_{O_2}^m$ and H_{H_2}, H_{O_2} are coefficient, the values are presented in the Table 1.

Table 1. Coefficients used in the calculation of the diffusion flow rates.

Coefficient	Value/Equation	Reference
$\boldsymbol{D_{H_2}^m}$	$13.1 \cdot 10^{-9}\ \frac{m^2}{s}$	[56]
$\boldsymbol{D_{O_2}^m}$	$5.7 \cdot 10^{-9}\ \frac{m^2}{s}$	[56]
$\boldsymbol{H_{H_2}}$	$\frac{1}{0.255 \cdot 10^5 \cdot exp\left(\frac{170}{T}\right) \cdot 101325 \cdot 10^{-6}}$	[57]
$\boldsymbol{H_{O_2}}$	$\frac{1}{1.33 \cdot 10^6 \cdot exp\left(\frac{-666}{T}\right) \cdot 101325 \cdot 10^{-6}}$	[58]

To calculate the flow of the total produced hydrogen, the following formula is used:

$$\dot{n}_{H_2}^{produced} = \frac{I_{el}}{2 \cdot F} - \dot{n}_{H_2}^{a} - 2 \cdot \dot{n}_{O_2}^{c} \tag{13}$$

The hydrogen concentration in oxygen (anodic ratio) can be expressed as:

$$y_{H_2}^{a} = \frac{\dot{n}_{H_2}^{a}}{\frac{i}{4 \cdot F} - \dot{n}_{O_2}^{c}} \cdot 100 \tag{14}$$

In order to ensure that the hydrogen concentration does not reach the lower flammability limit (LFL), it is required to create a condition in the MATLAB code. As per Schalenbach et al. [15] and Babic et al., [59] the Anodic Hydrogen Content must not exceed 2 $vol\%\ H_2$.

3. 2. Compressor model

The compressor power is calculated as [59]:

$$Power_{comp} = \frac{\gamma}{\gamma - 1} \frac{RT}{\eta_{comp}} \left[\left(\frac{P_{H_2}^{del}}{P_{H_2}^{c}} \right)^{\frac{\gamma}{\gamma - 1}} - 1 \right] \cdot \dot{n}_{H_2}^{produced} \tag{15}$$

where the efficiency of compressor is $\eta_{comp} = 80\%$. And $\gamma = 1.41$ is the isentropic expansion factor.

3. 2. Economic model of Levelized cost of hydrogen

In order to calculate the total cost of hydrogen, the following assumptions were made:

CAPEX of the electrolyzer	$1500\ \frac{€}{kWh}$ [62]
OPEX of the electrolyzer	3% of CAPEX of the electrolyzer per year [16]
Lifetime (LT) of the electrolyzer	10 years or ~80000 hours [16]
CAPEX of the compressor	$3800\ \frac{€}{kW}$ [61]
OPEX of the compressor	3% of CAPEX of the compressor per year [16]
The price of electricity	$0.12\ \frac{€}{kWh}$ [60]

Taking the previous assumptions into account, the levelled cost of hydrogen $LCOH_{H_2}$ can be calculated as [3]:

$$LCOH_{H_2} = \frac{CAPEX_{el}\left[\frac{€}{m^2}\right] + CAPEX_{comp}\left[\frac{€}{m^2}\right] + OPEX_{el}\left[\frac{€}{m^2}\right]}{H_{2_{produced}}^{total}} + \frac{OPEX_{comp}\left[\frac{€}{m^2}\right] + P_{el}^{cost}\left[\frac{€}{m^2}\right] + P_{comp}^{cost}\left[\frac{€}{m^2}\right]}{H_{2_{produced}}^{total}} \quad (16)$$

where $H_{2_{produced}}^{total}$ is the amount of hydrogen produced during the lifetime of the electrolyzer and it is calculated as :

$$H_{2_{produced}}^{total} = \dot{n}_{H_2}^{produced} \cdot M_{H_2} \cdot LT_{el} \quad (17)$$

where $M_{H_2} = 2.016 \cdot 10^{-3}\left[\frac{kg}{mol}\right]$ is the molar mass of hydrogen. The unit in which total hydrogen produced $H_{2_{produced}}^{total}$ is express in is $\left[\frac{kg}{m^2}\right]$ and the lifetime of the electrolyzer is converted into $[s]$.

CAPEX of the electrolyzer is calculated with the equation below:

$$CAPEX_{el}\left[\frac{€}{m^2}\right] = CAPEX_{el}\left[\frac{€}{Wh}\right] \cdot Power_{el} \cdot LT_{el} \quad (18)$$

Usually, to calculate the CAPEX the nominal power is used, as it provides a standardized and consistent basis for comparing different electrolyzer technologies and sizes. This is true for the comparison of electrolyzers with the same pressure output but for the different pressure values it is strictly necessary for the CAPEX to be dependent on the said output pressure to compare these electrolyzers adequately. The nominal power does not depend on the pressure, so it cannot be used for such a comparison, while the consumed power depends on the optimal current, which depends on the electrolyzer pressure. As for now, there is no agreed way of CAPEX calculations for electrolyzers with different outlet pressures, so the assumption of using the consumed power has been made. As a result, in equation of electrolyzer CAPEX (18), the power consumed by the electrolyzer (10) is used.

Similarly, CAPEX of compression calculated as follows:

$$CAPEX_{comp}\left[\frac{€}{m^2}\right] = CAPEX_{comp}\left[\frac{€}{Wh}\right] \cdot Power_{comp} \cdot LT_{comp} \quad (19)$$

The OPEX is a cost of maintenance, 3% of CAPEX is contributed for maintenance yearly for both electrolyzer and compressor:

$$OPEX_{el}\left[\frac{€}{m^2}\right] = CAPEX_{el}\left[\frac{€}{m^2}\right] \cdot 3\% \cdot \frac{LT_{el}}{365 \cdot 24} \quad (20)$$

$$OPEX_{comp}\left[\frac{€}{m^2}\right] = CAPEX_{comp}\left[\frac{€}{m^2}\right] \cdot 3\% \cdot \frac{LT_{comp}}{365 \cdot 24} \quad (21)$$

The cost of power consumed by the electrolyzer P_{el}^{cost} and the cost of power consumed by the compressor P_{comp}^{cost} can be calculated as:

$$P_{el}^{cost} = P_{el} \cdot lifetime_{el} \cdot electricity\ price \quad (22)$$

Similarly, for the compressor:

$$P_{comp}^{cost} = P_{comp} \cdot lifetime_{comp} \cdot electricity\ price \tag{23}$$

4. Results and discussion

In the pursuit of optimizing compression of hydrogen with a balance between the electrochemical compression and mechanical compression with a primary focus minimizing the overall cost of hydrogen production, our investigation delves into a comprehensive parametric study utilizing Proton Exchange Membrane (PEM) electrolyzers and high-pressure compressors. After performing the parametric study, optimization of these parameters is performed.

4. 1. Parametric study

This section presents a meticulous analysis of the interplay between various operational parameters and their impact on the production of high-pressure hydrogen. Examining parameters are anodic ratio, efficiency, cell voltage, and levelized cost of hydrogen (LCOH). We aim to unravel the intricate dynamics that govern the interplay of these parameters. Through a systematic exploration of these variables, our findings provide valuable insights into optimizing the PEM electrolysis process and subsequent compression, paving the way for enhanced efficiency and reliability in high-pressure hydrogen generation.

(a)

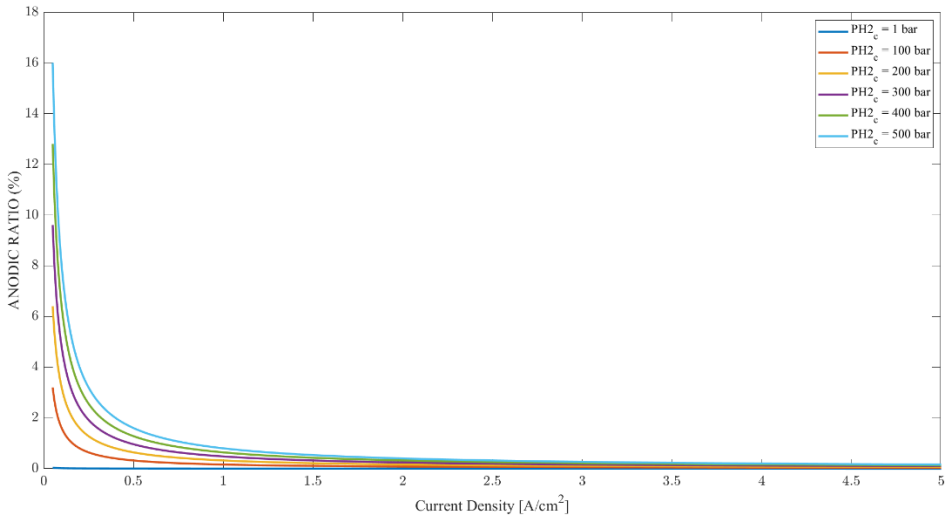

(b)

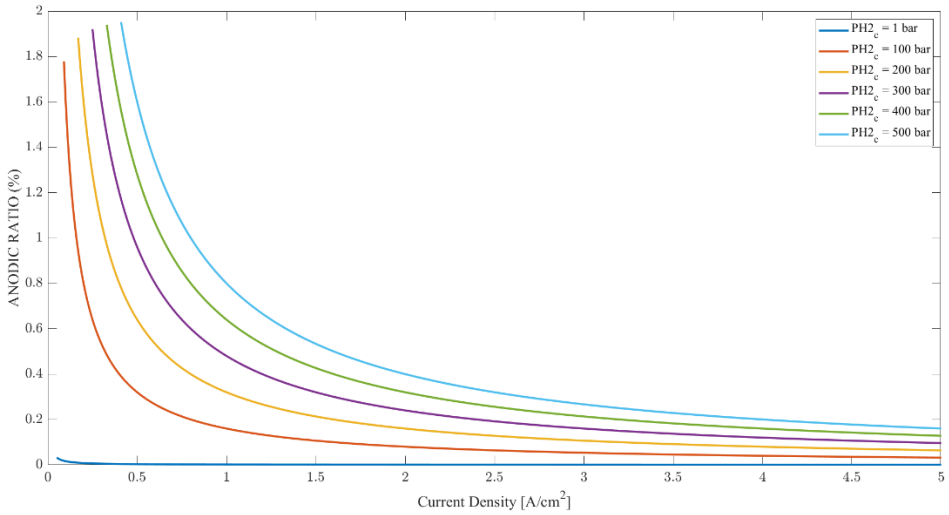

Figure 10. Anodic Ratio vs Current Density for a different value of Intermediate Pressure: (a) without 2% limitation, (b) with 2% limitation implemented.

Comparing Fig. 10 (a) with Fig. 10 (b), by not restricting the anodic ratios to lower than 2%, its value ranges between 3% to 16% for pressure of 100 bar and 500 bar, respectively. This substantial variation raises severe safety concerns as highlighted in the literature review. This result is a serious reminder to constrain the anodic ratios under 2% to prevent any explosions. In Fig. 10 (b), a noticeable trend emerges as the current density increases: the anodic ratio consistently decreases across all different electrolyzer pressures with higher current densities. This variation is due to the fact that the greater the current density, the greater the flow of oxygen, thus diluting the hydrogen that has passed through the membrane. This phenomenon could be attributed to the enhanced mass transport of reactants and products at higher current densities, thereby reducing the overpotential required for oxygen evolution compared to hydrogen evolution. Notably, a higher intermediate pressure correlates with a higher anodic ratio at the same current density. This observation be because higher electrolyzer pressures (intermediate pressures) may induce changes in gas solubility, diffusion rates, and mass transport phenomena, influencing the local concentration of reactants and thus altering the kinetics of the electrochemical reactions at the anode. These alterations could contribute to an increase in the diffusion of hydrogen across the membrane in comparison to the evolution of the oxygen from the cathode.

Fig. 11 represents the effect of different membrane thicknesses on anodic ratio as the current density increases.

(a)

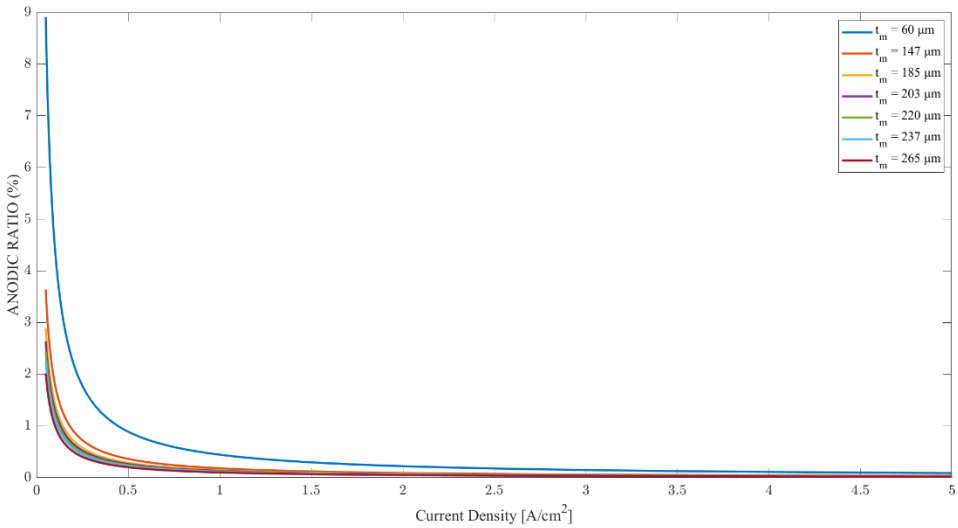

(b)

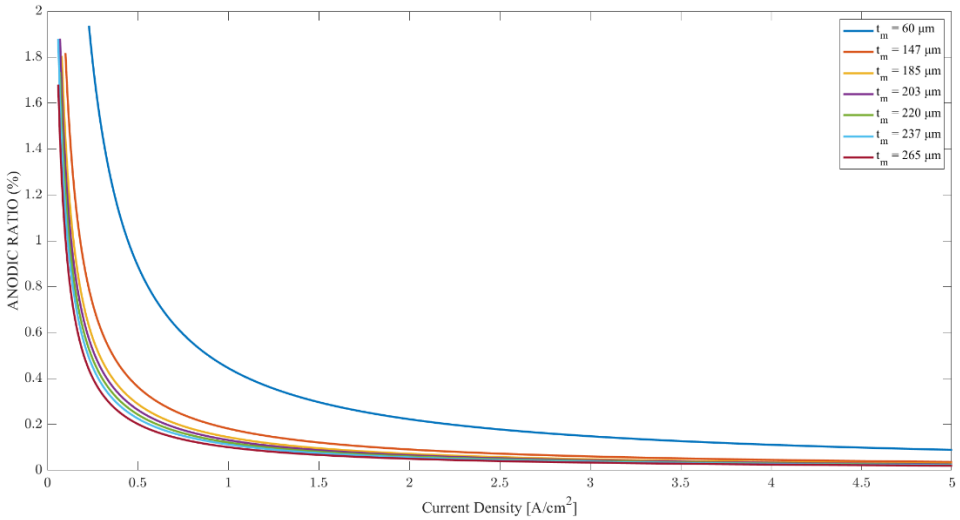

Figure 11. Anodic Ratio vs Current Density for a different value of Membrane Thickness: (a) without 2% limitation, (b) with 2% limitation implemented

Similar to Fig. 10, not limiting the anodic ratios to lower than 2%, safety concerns may arise for different membrane thickness. In Fig. 11 (b), it can be seen that as the current density increases, the anodic ratio decreases for all different membrane thicknesses. This phenomena attributes to several interconnected electrochemical and transport phenomena within the PEM electrolyzer system. As current density rises, the electrochemical reactions at the anode become more pronounced, leading to an accelerated rate of hydrogen ion generation which results in an increased concentration of protons near the anode interface. Moreover, as the current density escalates, mass transport limitations may become more prominent. Furthermore, the diffusion of reactants, such as water molecules and protons, from the bulk of the electrolyte to the anode may struggle to keep pace with the heightened electrochemical demand. This can lead to a localized depletion of reactants near the anode. Additionally, Fig. 11, indicates that at a constant current density, anodic ratio decreases with thicker membranes. As the membrane thickness rises, the distance that ions must traverse within the membrane also increases, resulting in higher electrical resistances. This elevated ohmic resistance can lead to voltage losses, diminishing the efficiency of the electrochemical reactions at the anode and subsequently reducing the anodic ratio. Moreover, thicker membranes may introduce additional diffusion limitations. The extended path length for the transport of protons and water molecules through the membrane can slow down the rate at which reactants reach the anode, causing concentration polarization effects. This, in turn, hampers the electrochemical reactions and contributes to a decrease in the anodic ratio. These insights underscore the delicate balance required in optimizing membrane thickness to achieve optimal performance in PEM electrolyzer systems.

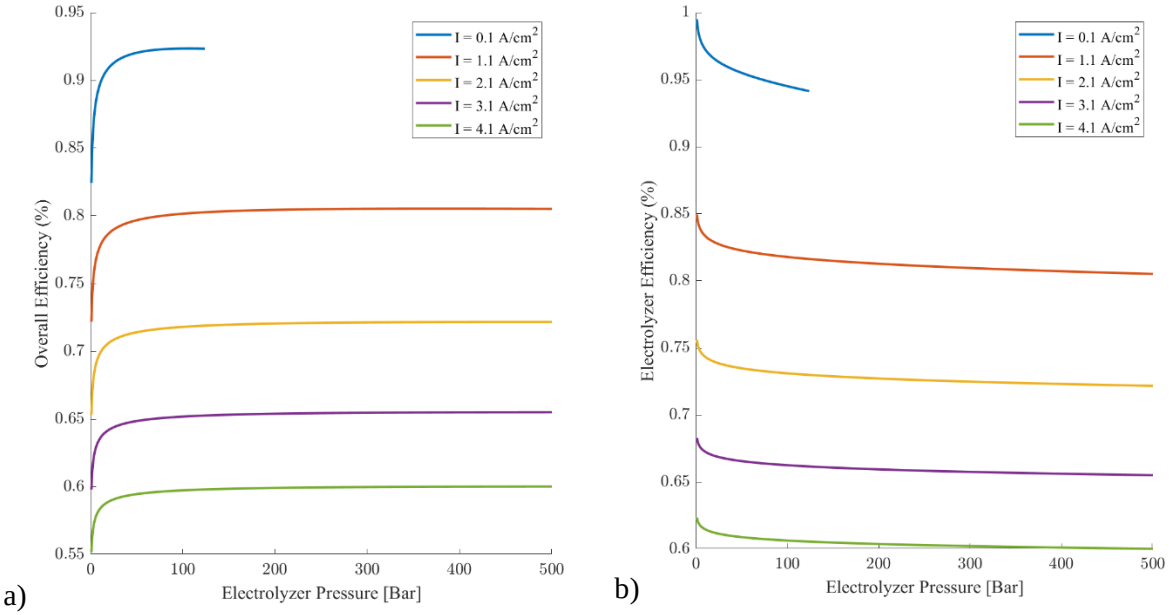

Figure 12. Efficiency vs Intermediate Pressure at T= 60ºC and t_m= 265 µm for a different value of Current Density: (a) Overall Efficiency, (b) Electrolyzer Efficiency

Fig. 12 (a) represents the dependence of the overall efficiency on the electrolyzer (intermediate) pressure, while the Fig. 12 (b) represents the dependence of the electrolyzer efficiency on the electrolyzer pressure, both for different values of current densities. Taking a brief look and comparing these two figures, It can clearly be seen that both the overall and electrolyzer efficiencies have higher values for lower values of current density. However, for a constant current, overall efficiency is increasing with higher values of intermediate pressure, while the electrolyzer efficiency behaves the opposite, it decreases with higher intermediate pressure. From the Fig. 12 (a) it can be seen that the slope of the graph is much steeper for the values until around 20 bar. It can be seen the reason for this from the Fig. 13, where the compressor pressure ratio and compressor power are expressed as a function of the intermediate pressure. Here, the compressor ratio decreases faster for the intermediate pressures under 20 bar. Mathematically speaking, the function of the compressor pressure ratio is a hyperbola, which means that the compressor ratio is inversely proportional to the intermediate pressure. This phenomena explains why the overall efficiency increases despite the decrease in electrolyzer efficiency. Higher compression ratio means more power (electricity) consumed by the compressor. Hence, this steep decrease in compressor ratio explains the steep increase in overall efficiency. For higher values of intermediate pressure, the changes do not happen as fast, which explains why the slope is not as steep. Another important observation is for the current density of $i = 0.1 \frac{A}{cm^2}$. For values of intermediate pressure higher than 130 bar, the curve suddenly flattens for both graphs. The reason for this can be found in anodic ratio because the production of hydrogen is directly proportional to the electrolyzer pressure. Higher the electrolyzer pressure, higher the hydrogen production which results in higher anodic ratio. However, anodic ratio is inversely proportional to the current density, hence why for low current densities we are obtaining higher anodic ratios.

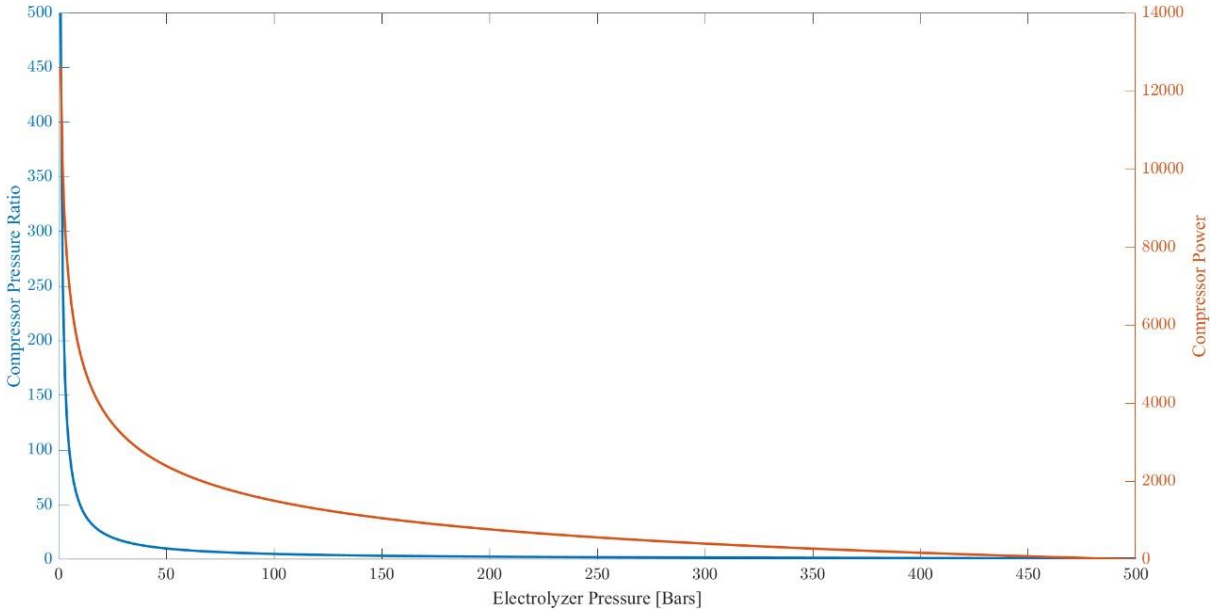

Figure 13. Compressor pressure ratio vs electrolyzer pressure at T= 60ºC and t_m= 265 µm

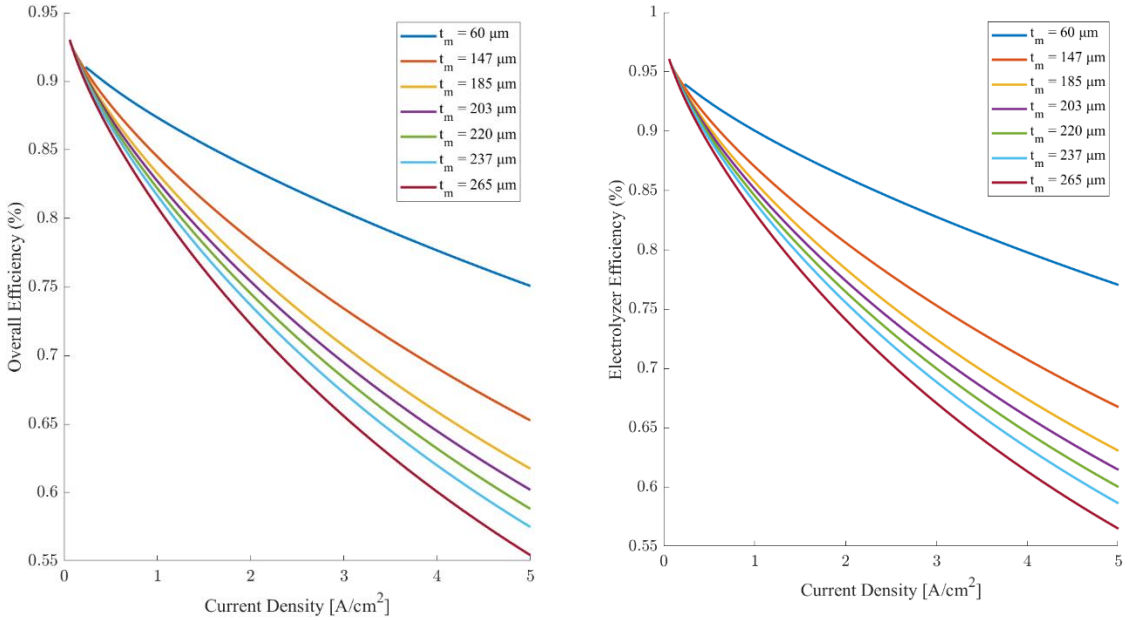

Figure 14. Efficiency vs Current Density at T= 60ºC and P= 62 bar for a different value of Membrane Thickness: (a) Overall Efficiency, (b) Electrolyzer Efficiency

To understand the effect of current density on efficiencies, Fig. 14 is plotted at different membrane thicknesses. As it can be seen in Fig. 14, both overall and electrolyzer efficiencies decreases with a similar trend as the current density increases at all membrane thicknesses. At higher current densities, the electrochemical reactions at the anode and cathode become more demanding, leading to increased overpotentials. Overpotentials are the extra voltage required to drive the desired electrochemical reactions, and they contribute to energy losses. As current density rises, the overpotentials at both electrodes increase, resulting in a higher overall energy input to sustain the electrolysis process. Moreover, higher current densities exacerbate concentration polarization effects. The rapid consumption of reactants at the electrodes, coupled with limited mass transport, can create localized depletion zones near the electrode surfaces, reducing reaction rates and efficiency. However, the rate of efficiency reduction for thicker membranes is larger compared to thin membranes. Thicker

membranes generally introduce higher ohmic losses due to the increased distance ions must traverse within the membrane. As current density rises, these higher ohmic losses in thicker membranes become more pronounced, leading to a more significant reduction in efficiency compared to thinner membranes. In addition, The extended path length in thicker membranes can exacerbate diffusion limitations. At higher current densities, the demand for reactants at the electrodes intensifies. Thicker membranes may struggle to facilitate rapid and efficient mass transport, resulting in a more substantial decrease in efficiency compared to thinner membranes.

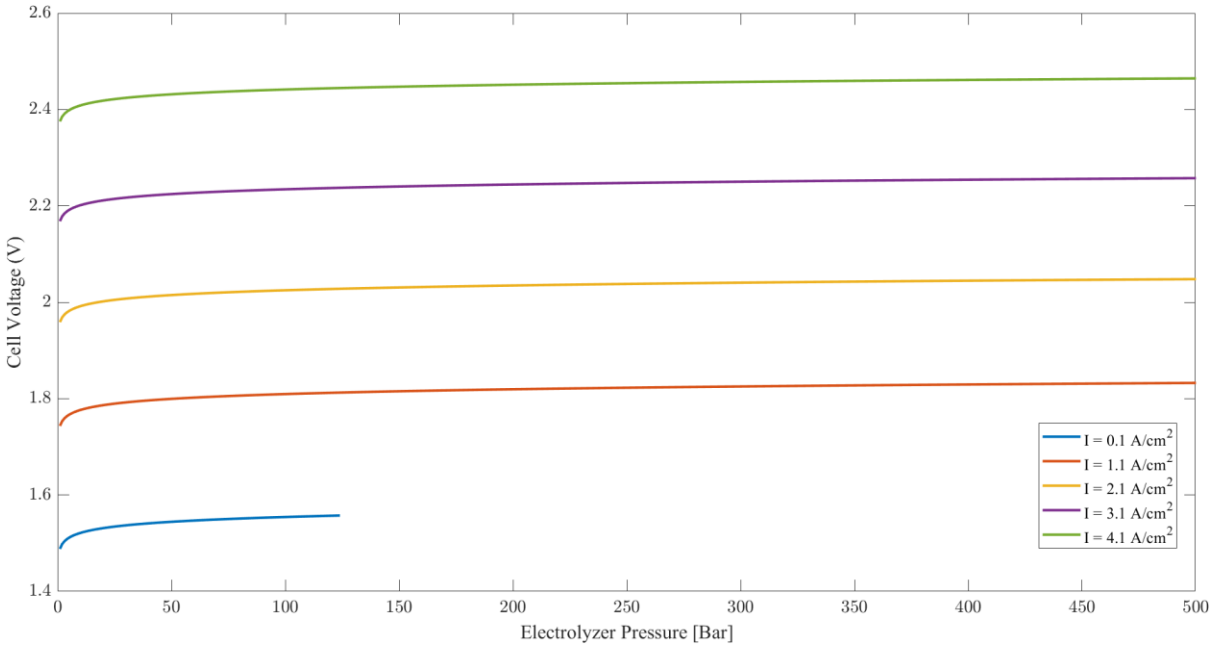

Figure 15. Cell voltage vs electolyzer pressure at T= 60ºC and t_m= 265 µm for different values of current density

As illustrated in Fig. 15, cell voltage slightly increases with electrolyzer pressure. On the other hand, at a constant electrolyzer pressure, higher current densities results in higher cell voltages. As the current density increases, the ohmic losses within the electrolyte and electrodes become more pronounced. Ohmic losses are directly proportional to the current passing through the system, and they contribute to the overall voltage drop across the cell. Therefore, higher current densities result in higher ohmic losses and an associated increase in cell voltage. The reason that the line for current density = 0.1 A/cm^2 does not extends after a certain electrolyzer pressure is the anodic ratio exceeds 2% since increasing pressure increases anodic ratio, as seen in Fig. 10.

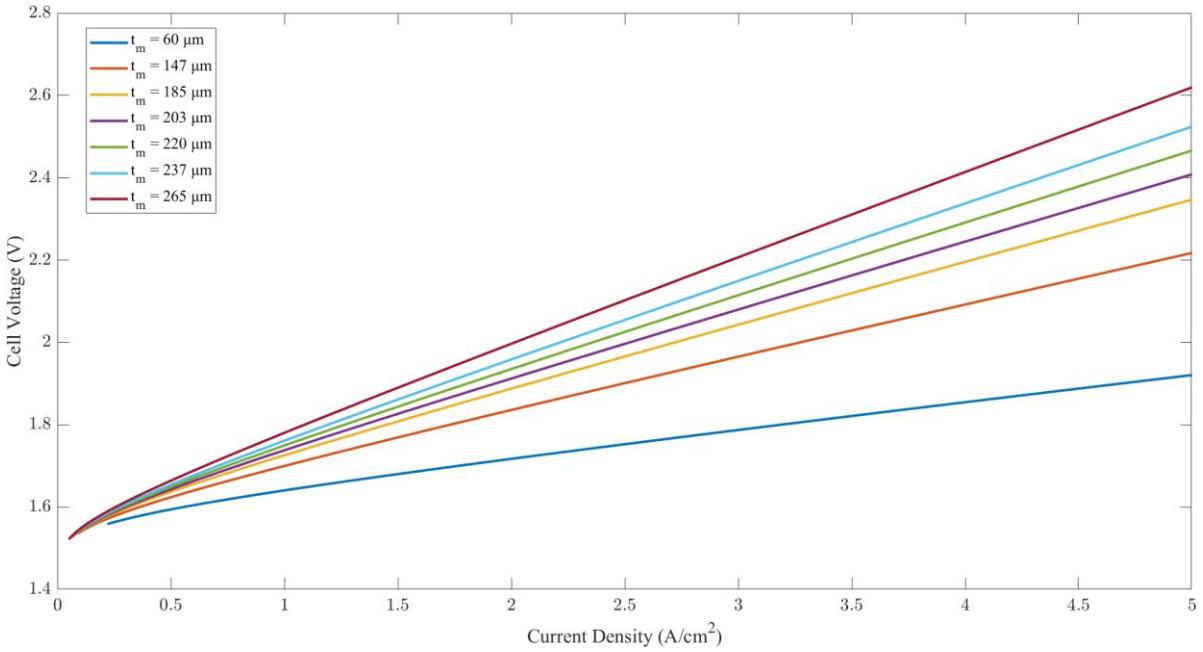

Figure 16. Cell voltage vs current density at T= 60ºC and P= 62 bar for different values of membrane thickness

Similar to Fig. 15, it can be seen in Fig. 16 that with an increase in current density, the cell voltage rises. Furthermore, at a constant current density, thicker membrane attributes to higher cell voltage. Firstly, the additional distance that ions must traverse within the thicker membrane leads to higher electrical resistances. Consequently, the ohmic losses contribute to a higher voltage drop across the cell. Secondly, thicker membranes can exacerbate mass transport limitations and introduce higher diffusion resistance. The extended path length for the transport of reactants through the thicker membrane can impede the efficient movement of ions and molecules, leading to concentration polarization effects. This limitation in mass transport can contribute to an elevation in cell voltage.

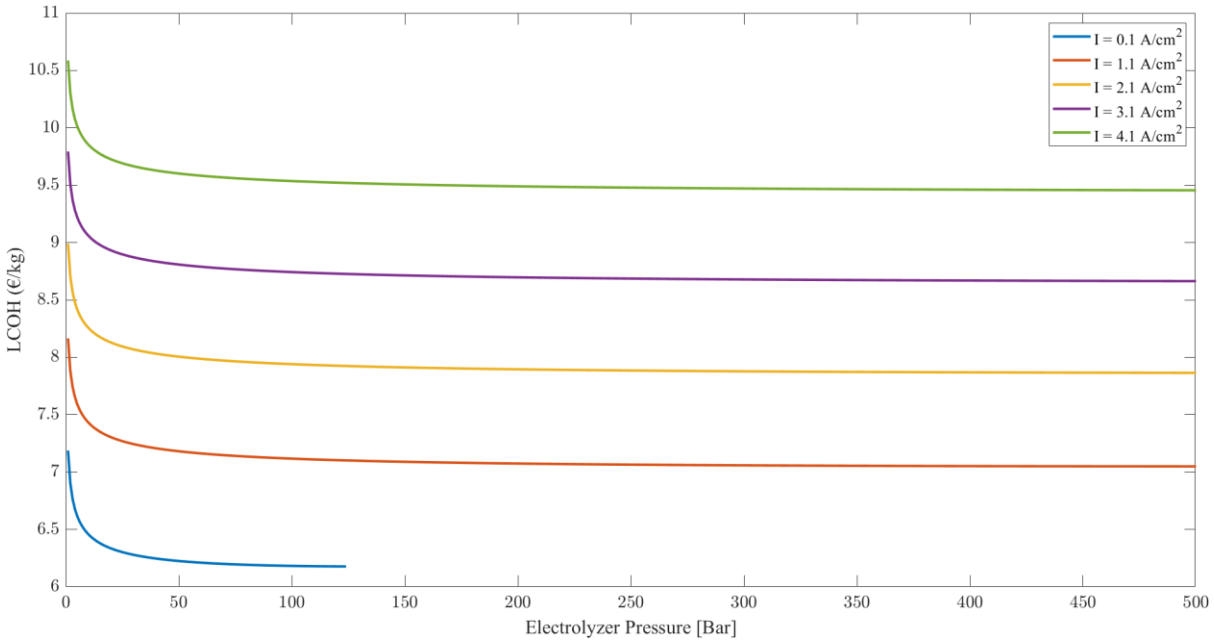

Figure 17. Levelized cost of hydrogen (LCOH) vs electolyzer pressure at T= 60ºC and t_m= 265 µm for different values of current densities.

As shown in Fig. 17, the LCOH decreases as the electrolyzer pressure increases up to the 62 bar and then stays approximately constant. In addition, increasing current density will increase the LCOH at a constant pressure. The main reason is that higher current densities generally result in increased energy consumption during electrolysis. This heightened demand for electrical energy contributes to higher operating costs, impacting the overall LCOH.

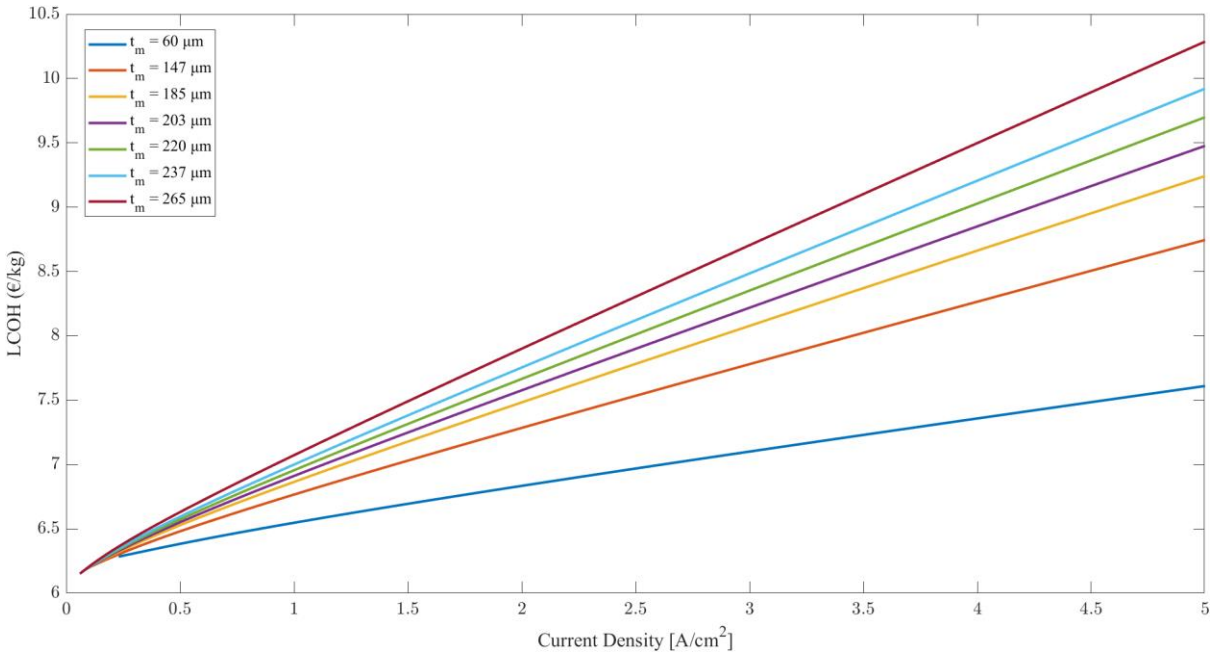

Figure 18. levelized cost of hydrogen (LCOH) vs current density = 60ºC and P= 62 bar for different values of membrane thickness

Fig. 18 shows a the relationship between current density and the LCOH. It is clear that with an increase in current density, the LCOH increases correspondingly. This relationship was investigated for 7 different standard Nafion membrane thicknesses (60, 147, 185, 203, 220, 237, 265 (µm)). It was observed that thicker Nafion membranes had higher LCOH for the same current density. However, it is imperative to highlight that in the electrolyzer design for each membrane thickness, the current density used should ensure that the anodic ratio is less than 2%. Typically, higher current density ensure a lower anodic ratio as previously highlighted in the description for Fig. 10. Moreover, the lower LCOH observed at lower current densities is a consequence of the lower power at lower current densities and this is described more in detailed in the preceding section.

4. 2. Optimisation

After the parameter study and understanding the behaviour of different variables, a code in MATLAB is developed to find the optimised current density, electrolyzer pressure, and membrane thickness for compression of hydrogen to minimize the LCOH.

First, the optimum membrane thickness is calculated so the rest of the optimization studies is performed at this thickness. The result for this optimization is presented at Fig. 19.

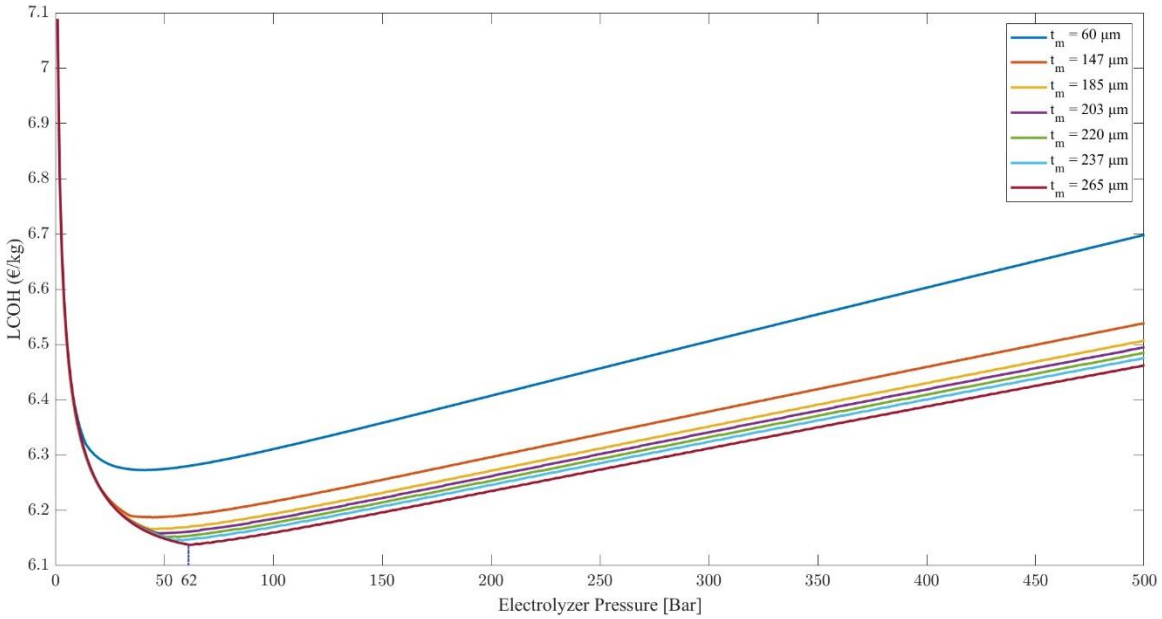

Figure 19. LCOH vs electolyzer pressure at T= 60ºC for different membrane thickness

The studied membrane thicknesses are chosen due to the commercial membranes available in the market. As seen in Fig. 19, at each intermediate pressure, the minimum LCOH is achieved with the thickest membrane. Thicker membrane enables the electrolyzer to work at lower current densities with respect to 2% anodic ratio (Fig. 11). This lower current density significantly reduces the cost due to the electricity consumption which plays a dominant role in LCOH (see orange line in Fig. 20). Consequently, thicker membranes involve higher initial capital costs, but at intermediate pressures the reduction of operational costs result in an overall minimum LCOH for systems employing thicker membranes.

Moreover, at the thickest membrane (265 µm) the minimal LCOH is reached at 62 bar. More comprehensive study on this point requires a more detailed breakdown of LCOH which is presented in Fig. 20.

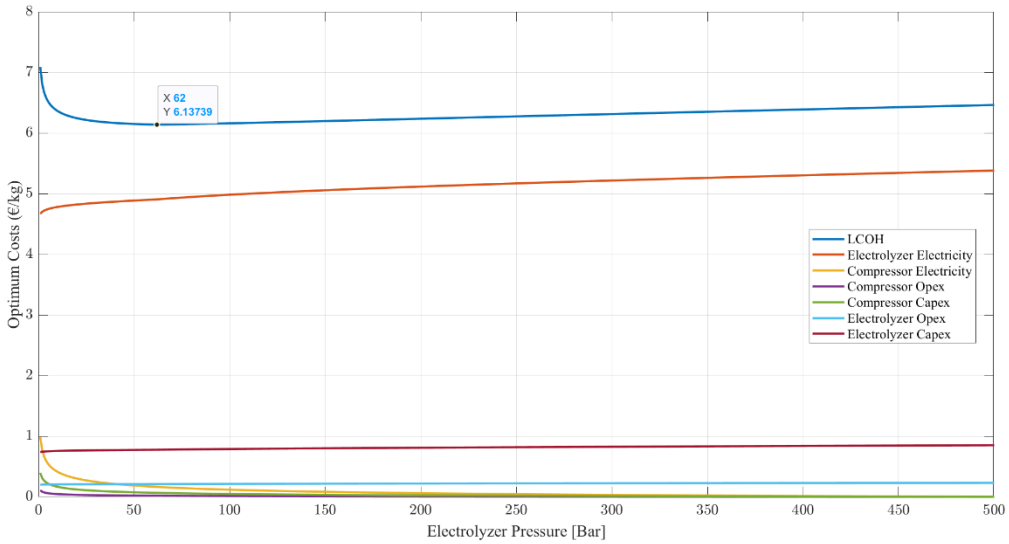

Figure 20. Levelized Cost of Hydrogen (LCOH) vs Electrolyzer Pressure for 265 µm membrane thickness

Fig. 20 summarizes an investigation carried out to minimize the LCOH by optimizing the intermediate pressure using a design thickness of 265 µm found to be the most optimal in Fig. 19. By taking a look at Fig. 20 it is clear that an intermediate pressure of 62 bar minimizes the LCOH. Here, of great significance is how the LCOH first decreases rapidly, exponentially up to the optimal pressure point before steadily increasing in linear fashion. This increase in the electrolyzer electricity can be explained by referring to Fig. 21, which shows that an increase in intermediate pressure results in an increase in optimum current density (to minimize the anodic ratio below 2 % for safety), hence leading to a corresponding increase in power.

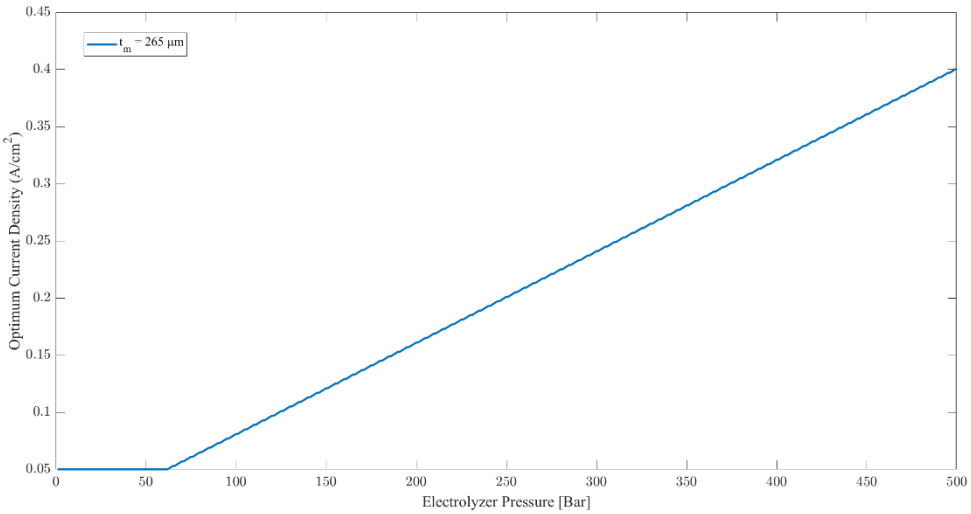

Figure 21. Optimum current density vs electrolyzer pressure at T= 60ºC and t_m= 265 µm

From the Fig. 20 it is clear that the biggest part of this LCOH is electrolyzer electricity at all investigated electrolyzer pressure up to 500 bar. Over this pressure range, the electrolyzer consumed electricity is seen to rise with increasing electrolyzer pressure. The third most significant part of the LCOH is the Electrolyzer Capex which increases fairly steadly over the various intermediate pressures. The small increase on the electrolyzer capex andelectricyti cost with the decrease of all the compressor costs over intermediante pressure lead to the optimal point of 62 bar. Moreover, the electrolyzer Opex and the compressor Opex are seen to be insignificant since the Opex is only 3% of the Capex yearly, as highlighted in the literature. At higher intermediate pressures, we also observe that the compressor

Capex and Opex falling to 0 at 500 bar due to the decrease in the pressure ratio since a compressor will not be needed at that point. The investigation highlights the pivotal role of optimizing intermediate pressure, particularly at 62 bar in minimising the LCOH in PEM electrolyzer systems, offering valuable insights for cost-effective and safe hydrogen production.

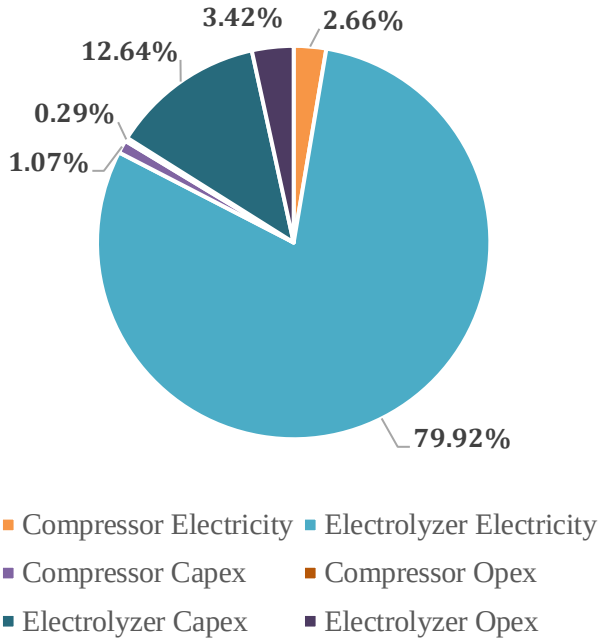

Figure 22. Breakdown of LCOH for optimized parameters at T= 60ºC, t_m= 265 µm and P= 62 bar

Fig 22. shows the breakdown of LCOH for optimized parameters. It can be seen that the electrolyzer electricity cost makes a major share of LCOH. Around 80% percent of the cost to produce 1 kg of hydrogen is being used to pay the electricity bill. Therefore, it is important to procure or produce the electricity at cheaper rates, as economic viability of producing hydrogen using an electrolyzer highly depends on it. The detailed imapct of electricity prices on LCOH is shown in Fig. 23.

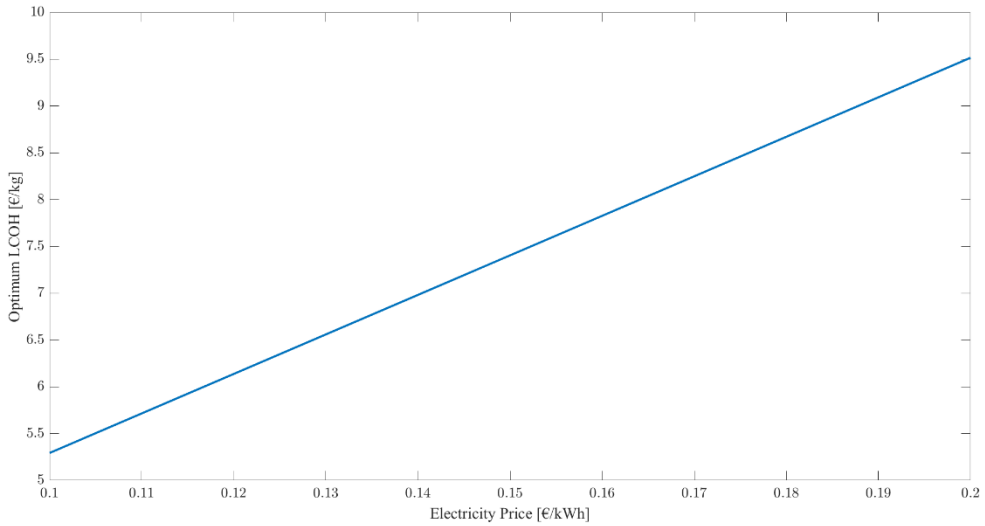

Figure 23. Optimum LCOH vs Electricity price at T= 60ºC, t_m= 265 µm and P= 62 bar

The linear relationship observed in Fig. 22 between electricity price and Optimum LCOH at an operating pressure of 62 bar is a critical indicator in energy systems planning and investment. This

relationship demonstrates how changes in electricity prices directly impact the overall cost of hydrogen production. Such insights are invaluable for feasibility studies conducted by different countries or regions aiming to assess the viability of hydrogen as a long-term energy carrier for storing intermittent renewable energy generated by sources like wind and solar. The graph serves as a practical reference tool allowing stakeholders to anticipate the economic feasibility of hydrogen production under varying electricity price scenarios. By understanding how electricity price influences optimum LCOH, decision makers can make informed choices regarding energy storage and transition strategies, thereby facilitating the integration of hydrogen into future energy systems.

4. 3. Economic viability of direct electrochemical compression

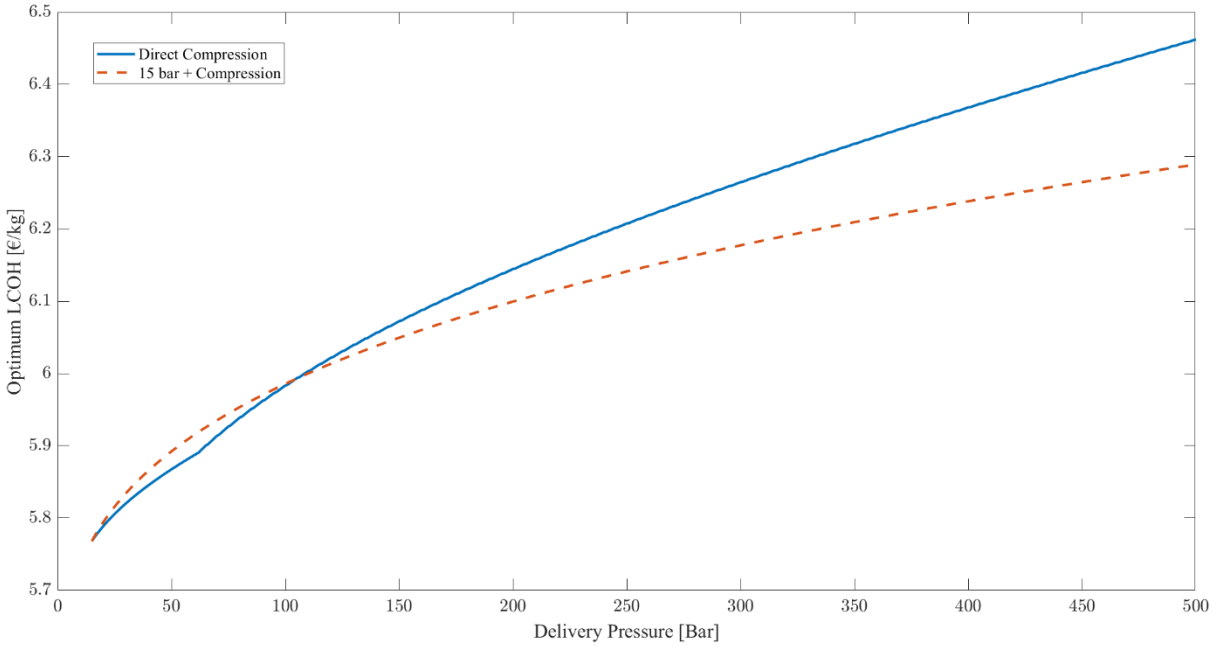

Figure 24. Optimum LCOH vs delivery pressure for direct compression and dual electrochemical compression to 15 bar and mechanical compression

In Fig. 23 the impact of delivery pressure on optimum LCOH has been analysed for the electricity price of 0.12 €/kWh. Two cases have been presented in Fig. 23. In first case (solid blue line) only the electrolyzer has been used to achieve the desired delivery pressure, while in the second case (dotted red line) first the electrolyzer has been used to compress hydrogen up to 15 bars and then a compressor has been used to achieve the desired delivery pressure. Analysing both cases, we can clearly see that up to around 100 bars it is more economical to compress the gas directly using the electrolyzer, and only above that, using the compressor becomes economical. From Fig. 13, it is clear that compressor power is highly dependent on the compression ratio, and as the result, an exponential increase in compressor for the delivery pressures up to 100 bar is seen, and afterwards the trend is almost steady, while electrolyzer power increases steadily. After the 100-bar point, the compressor power stabilizes, while electrolyzer power keeps rising, resulting in higher LCOH for direct compression.

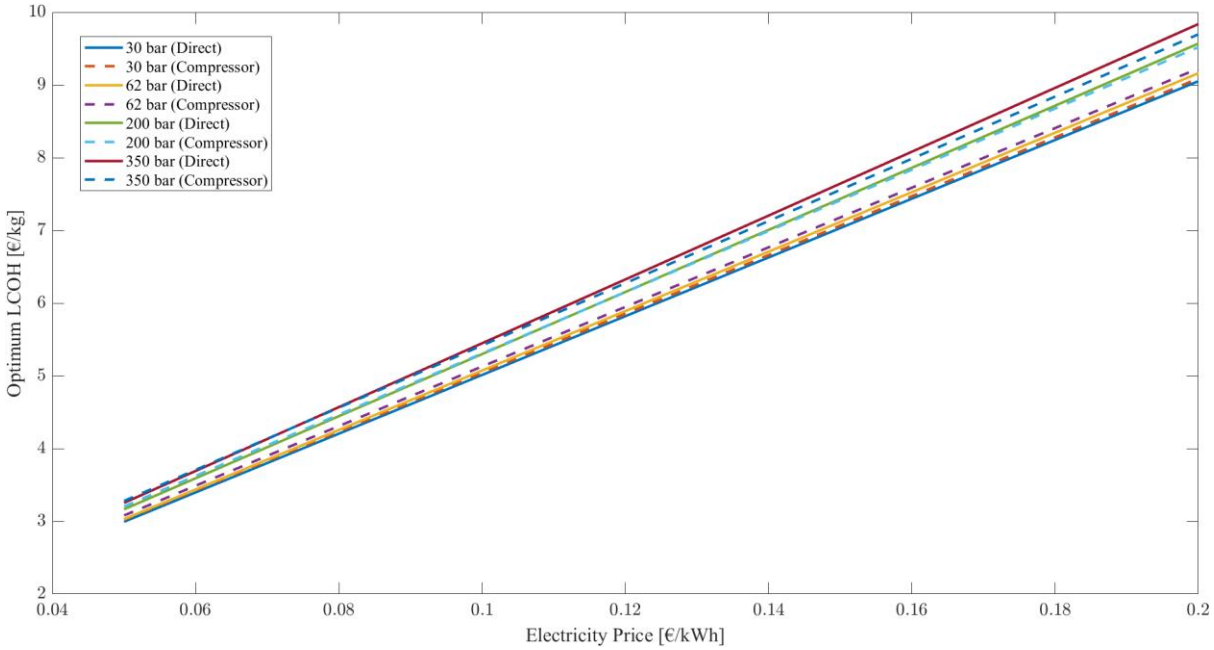

Figure 25. Optimum LCOH vs eletricity price

In Fig. 25 the impact electricity prices is shown on optimum LCOH for various delivery pressures. Again, the two cases have been presented in Fig. 24. Solid lines represent the case of direct compression using only the electrolyzer while the dotted lines represent the case with using the electrolyzer up to 15 bar and then using the compressor to achieve the desired delivery pressure. It can be seen that whether it is economical to compress the gas directly using the electrolyzer or using the compressor highly depends on the electricity price. The lower the price for electricity, the less the need to implement a compressor to achieve the desired delivery pressures. For instance, even the higher pressure like 200 bar becomes economically feasible to achieve using only the electrolyzer when the electricity price reaches 0.05 €/kWh.

5. Conclusion

In line with the European Union's objectives to mitigate global warming and enhance energy independence, the utilization of green hydrogen has emerged as a pivotal solution. The projected increase in green hydrogen constituting 24% of final energy consumption in Europe by 2050 underscores the imperative for its efficient production. In this regard, hydrogen pressurization plays a pivotal role in the storage and transportation of hydrogen. To minimize the overall cost of hydrogen production, this research focuses on optimizing electrochemical compression with a primary focus on producing high-pressure hydrogen. Proton exchange membrane (PEM) electrolysis stands out as a technology capable of producing hydrogen at high pressure compared to other technologies, thereby potentially reducing the need for making use of higher compression ratios.
Integration of the PEM electrolyzer and hydrogen compressor is modelled in MATLAB code to optimize the intermediate pressure, current density, and membrane thickness. To understand the complicated interplay of multiple parameters a parametric study is done. The eminent results of this part are:

- Restricting the anodic ratio is essential as it can increase up to 16% which raises serious safety concerns.
- The anodic ratio consistently decreases across all different electrolyzer outlet pressures with higher current densities.
- As the current density increases, the anodic ratio decreases for all different membrane thicknesses.
- At a constant current density, the anodic ratio decreases with thicker membranes.
- Both the overall and electrolyzer efficiencies have higher values for lower values of current density.
- While, for a constant current overall efficiency is increasing with higher values of intermediate pressure, electrolyzer efficiency decreases.
- At a constant electrolyzer pressure, higher current densities result in higher cell voltages.
- At constant pressure, increasing current density will increase the LCOH.
- It was observed that thicker Nafion membranes had higher LCOH for the same current density.

Then, by knowing the effect of change in each parameter, optimization of current density, electrolyzer pressure, and membrane thickness for compression of hydrogen to minimize the LCOH is performed, and the following results are achieved:

- The minimum LCOH is achieved with the thicker membrane (265 μm) since the thicker membrane enables the electrolyzer to work at lower current densities concerning a 2% anodic ratio. This lower current density significantly reduces the cost due to the electricity consumption which plays the most dominant role in LCOH.
- The biggest part of this LCOH is electrolyzer electricity. Since an increase in intermediate pressure results in an increase in optimum current density, leading to a corresponding increase in power consumption, an intermediate pressure of 62 bar minimizes the LCOH at the optimum membrane thickness.
- The linear relationship observed between electricity price and Optimum LCOH at the optimum operating pressure is a critical indicator in energy systems planning and investment. Such insights are invaluable for feasibility studies conducted by different countries or regions aiming to assess the viability of hydrogen as a long-term energy carrier.

The last insight in the optimization section drove the research to analyze the economic viability of direct electrochemical compression. It is found that for the electricity price of 0.12 €/kWh up to around 100 bars it is more economical to compress the hydrogen directly using the electrolyzer, and only above that, using the compressor is more economical. However, the electricity price heavily influences the economics of using the electrolyzer or the compressor to compress the gas directly. The lower the price for electricity, the less the need to implement a compressor to achieve the desired delivery pressures.

6. References

[1] IEA, *The Future of Hydrogen, IEA, Paris*. 2019, IEA, Paris.

[2] Abdin, Zainul, et al. "Hydrogen As an Energy Vector." *Renewable and Sustainable Energy Reviews*, vol. 120, 2020, p. 109620, https://doi.org/10.1016/j.rser.2019.109620

[3] Weidner, S., et al. "Feasibility Study of Large Scale Hydrogen Power-to-gas Applications and Cost of the Systems Evolving with Scaling up in Germany, Belgium and Iceland." *International Journal of Hydrogen Energy*, vol. 43, no. 33, 2018, pp. 15625-15638, https://doi.org/10.1016/j.ijhydene.2018.06.167

[4] Bhaskar, Abhinav, et al. "Decarbonization of the Iron and Steel Industry with Direct Reduction of Iron Ore with Green Hydrogen." *Energies*, vol. 13, no. 3, 2019, p. 758, https://doi.org/10.3390/en13030758

[5] Liu, Wenguo, et al. "The Production and Application of Hydrogen in Steel Industry." *International Journal of Hydrogen Energy*, vol. 46, no. 17, 2021, pp. 10548-10569, https://doi.org/10.1016/j.ijhydene.2020.12.123

[6] Zang, Guiyan, et al. "Technoeconomic and Life Cycle Analysis of Synthetic Methanol Production from Hydrogen and Industrial Byproduct CO2." Environmental Science & Technology, vol. 55, no. 8, 15 Mar. 2021, pp. 5248–5257, https://doi.org/10.1021/acs.est.0c08237

[7] Bellotti, D., et al. "Feasibility Study of Methanol Production Plant from Hydrogen and Captured Carbon Dioxide." *Journal of CO2 Utilization*, vol. 21, 2017, pp. 132-138, https://doi.org/10.1016/j.jcou.2017.07.001

[8] Moreno-Gonzalez, Marta, et al. "Carbon-neutral Fuels and Chemicals: Economic Analysis of Renewable Syngas Pathways via CO2 Electrolysis." *Energy Conversion and Management*, vol. 244, 2021, p. 114452, https://doi.org/10.1016/j.enconman.2021.114452

[9] Klell, M., Kindermann, H., Christian, J., (2007). Thermodynamics of gaseous and liquid hydrogen storage. In: Proceedings of IHEC 2007 the International Hydrogen Energy Congress and Exhibition, Istanbul, Turkey, 13–15 July. http://www.hycenta.tugraz.at/Image/Thermodynamics%20of%20gaseous%20and%20liquid%20hydrogen%20storage.pdf

[10] IRENA, Green Hydrogen Cost Reduction: Scaling up Electrolyzers to Meet the 1.5ºC Climate Goal. 2020, International Renewable Energy Agency: Abu Dhabi.

[11] IEA. (2023, July 10). Electrolyzers - Energy System. IEA. https://www.iea.org/energy-system/low-emission-fuels/electrolyzers

[12] Ayers, Katherine E., et al. Research Advances towards Low Cost, High Efficiency PEM Electrolysis. 2010, https://doi.org/10.1149/1.3484496

[13] Grigoriev, S.A., et al. "High-pressure PEM Water Electrolysis and Corresponding Safety Issues." *International Journal of Hydrogen Energy*, vol. 36, no. 3, 2011, pp. 2721-2728, https://doi.org/10.1016/j.ijhydene.2010.03.058

[14] Haryu, E., et al. "Mechanical structure and performance evaluation of high differential pressure water electrolysis cell." *Honda R&D Tech. Rev* 23.2 (2011).

[15] Schalenbach, Maximilian, et al. "Acidic or Alkaline? Towards a New Perspective on the Efficiency of Water Electrolysis." Journal of the Electrochemical Society, vol. 163, no. 11, 2016, pp. F3197–208, https://doi.org/10.1149/2.0271611jes

[16] Hancke, Ragnhild, et al. "The Case for High-pressure PEM Water Electrolysis." *Energy Conversion and Management*, vol. 261, 2022, p. 115642, https://doi.org/10.1016/j.enconman.2022.115642

[17] Hancke R, Ulleberg Ø, Bujlo P. High-Pressure PEM Water Electrolysis System. in EFCF2021. 2021, July 28. Zenodo

[18] El Kharbachi, A., et al. "Metal Hydrides and Related Materials. Energy Carriers for Novel Hydrogen and Electrochemical Storage." The Journal of Physical Chemistry C, vol. 124, no. 14, Apr. 2020, pp. 7599–607, https://doi.org/10.1021/acs.jpcc.0c01806

[19] Bellosta von Colbe, Jose, et al. "Application of Hydrides in Hydrogen Storage and Compression: Achievements, Outlook and Perspectives." *International Journal of Hydrogen Energy*, vol. 44, no. 15, 2019, pp. 7780-7808, https://doi.org/10.1016/j.ijhydene.2019.01.104

[20] Modi P, Aguey-Zinsou K-F. Room temperature metal hydrides for stationary and heat storage applications: a review. Front Energy Res 2021;9

[21] Dalena, Francesco, et al. "Advances in Methanol Production and Utilization, with Particular Emphasis toward Hydrogen Generation via Membrane Reactor Technology." *Membranes*, vol. 8, no. 4, 2018, p. 98, https://doi.org/10.3390/membranes8040098

[22] Jo, Young, and Bum J. Ahn. "Analysis of Hazard Area Associated with Hydrogen Gas Transmission Pipelines." *International Journal of Hydrogen Energy*, vol. 31, no. 14, 2006, pp. 2122-2130, https://doi.org/10.1016/j.ijhydene.2006.01.008

[23] Giddey, S., Badwal, S.P.S., Kulkarni, A. "Review of Electrochemical Ammonia Production Technologies and Materials." International Journal of Hydrogen Energy, vol. 38, no. 34, 2013, pp. 14576-14594. https://doi.org/10.1016/j.ijhydene.2013.09.054.

[24] Lord, Anna S., et al. "Geologic Storage of Hydrogen: Scaling up to Meet City Transportation Demands." International Journal of Hydrogen Energy, vol. 39, no. 28, 2014, pp. 15570-15582. https://doi:10.1016/j.ijhydene.2014.07.121.

[25] Crotogino, Fritz. "Chapter 20 - Larger Scale Hydrogen Storage." Storing Energy, edited by Trevor M. Letcher, Elsevier, 2016, pp. 411-429. ISBN 9780128034408. https://doi.org/10.1016/B978-0-12-803440-8.00020-8.

[26] Hydrogen Delivery Technical Team Roadmap. 2013. US Department of Energy: Office of Energy Efficiency & Renewable Energy.

[27] Rose, Philipp K., and Fabian Neumann. "Hydrogen Refueling Station Networks for Heavy-duty Vehicles in Future Power Systems." Transportation Research Part D: Transport and Environment, vol. 83, 2020, article 102358. https://doi.org/10.1016/j.trd.2020.102358.

[28] Schmidt, O., et al. "Future cost and performance of water electrolysis: an expert elicitation study." International Journal of Hydrogen Energy, vol. 42, no. 52, 2017, pp. 30470–92. https://doi.org/10.1016/j.ijhydene.2017.10.045.

[29] Hosseini, S. E., and M. A. Wahid. "Hydrogen from solar energy, a clean energy carrier from a sustainable source of energy." International Journal of Energy Research, vol. 44, no. 6, 2020, pp. 4110–31. https://api.semanticscholar.org/CorpusID:212906042

[30] Kumar, S. Shiva, and Hankwon Lim. "An Overview of Water Electrolysis Technologies for Green Hydrogen Production." *Energy Reports*, vol. 8, 2022, pp. 13793-13813, ISSN 2352-4847, https://doi.org/10.1016/j.egyr.2022.10.127.

[31] Guo, Xiaoqiang, et al. "Overview of Electrolyzer and Hydrogen Production Power Supply from Industrial Perspective." International Journal of Hydrogen Energy, vol. 49, no. C, 2024, pp. 1048-1059. ScienceDirect, https://doi.org/10.1016/j.ijhydene.2023.10.325

[32] Laguna-Bercero, M.A. "Recent advances in high temperature electrolysis using solid oxide fuel cells: A review." Journal of Power Sources, vol. 203, 2012, pp. 4-16. ISSN 0378-7753, https://doi.org/10.1016/j.jpowsour.2011.12.019.

[33] Nechache, A., Cassir, M., & Ringuedé, A. "Solid oxide electrolysis cell analysis by means of electrochemical impedance spectroscopy: A review." Journal of Power Sources, vol. 258, 2014, pp. 164-181. ISSN 0378-7753, https://doi.org/10.1016/j.jpowsour.2014.01.110.

[34] Shiva Kumar, S., & Himabindu, V. "Hydrogen production by PEM water electrolysis – A review." Materials Science for Energy Technologies, vol. 2, no. 3, 2019, pp. 442-454. ISSN 2589-2991, https://doi.org/10.1016/j.mset.2019.03.002.

[35] Carmo, Marcelo, et al. "A comprehensive review on PEM water electrolysis." International Journal of Hydrogen Energy, vol. 38, no. 12, 2013, pp. 4901-4934. ISSN 0360-3199, https://doi.org/10.1016/j.ijhydene.2013.01.151.

[36] Ito, H., Miyazaki, N., Ishida, M., & Nakano, A. (2016). Cross-permeation and consumption of hydrogen during proton exchange membrane electrolysis. International Journal of Hydrogen Energy, 41(45), 20439-20446. https://doi.org/10.1016/j.ijhydene.2016.08.119.

[37] Zawodzinski, T. A., Jr., Derouin, C., Radzinski, S., Sherman, R. J., Smith, V. T., Springer, T. E., & Gottesfeld, S. (1993). Water Uptake by and Transport Through Nafion® 117 Membranes. Journal of The Electrochemical Society, 140(4), 1041. https://doi.org/10.1149/1.2056194.

[38] Marangio, F., Pagani, M., Santarelli, M., & Calì, M. (2011). Concept of a high pressure PEM electrolyzer prototype. International Journal of Hydrogen Energy, 36(13), 7807-7815. https://doi.org/10.1016/j.ijhydene.2011.01.091.

[39] Omrani, Reza, and Bahman Shabani. "Hydrogen crossover in proton exchange membrane electrolyzers: The effect of current density, pressure, temperature, and compression." Electrochimica Acta, vol. 377, 2021, 138085, https://doi.org/10.1016/j.electacta.2021.138085

[40] Schalenbach, M., Carmo, M., Fritz, D. L., Mergel, J., & Stolten, D. (2013). Pressurized PEM water electrolysis: Efficiency and gas crossover. International Journal of Hydrogen Energy, 38(35), 14921-14933. https://doi.org/10.1016/j.ijhydene.2013.09.013.

[41] Schalenbach, M. (2016). Corrigendum to "Pressurized PEM water electrolysis: Efficiency and gas crossover" [Int J Hydrogen Energy 38 (2013) 14921–14933]. International Journal of Hydrogen Energy, 41(1), 729-732. https://doi.org/10.1016/j.ijhydene.2015.11.009.

[42] Schalenbach, M., & Stolten, D. (2015). High-pressure water electrolysis: Electrochemical mitigation of product gas crossover. Electrochimica Acta, 156, 321-327. https://doi.org/10.1016/j.electacta.2015.01.010.

[43] Vogt, H. (1980). On the supersaturation of gas in the concentration boundary layer of gas evolving electrodes. Electrochimica Acta, 25(5), 527–531. https://doi.org/10.1016/0013-4686(80)87052-6.

[44] Trinke, P., Haug, P., Brauns, J., Bensmann, B., Hanke-Rauschenbach, R., & Turek, T. (2018). Hydrogen crossover in PEM and alkaline water electrolysis: mechanisms, direct comparison and mitigation strategies. Journal of The Electrochemical Society, 165(7), F502–F513. https://doi.org/10.1149/2.0541807jes.

[45] Trinke, P., Bensmann, B., & Hanke-Rauschenbach, R. (2017). Current density effect on hydrogen permeation in PEM water electrolyzers. International Journal of Hydrogen Energy, 42(21), 14355–14366. https://doi.org/10.1016/j.ijhydene.2017.03.231.

[46] Klose, C., Trinke, P., Böhm, T., Bensmann, B., Vierrath, S., Hanke-Rauschenbach, R., & Thiele, S. "Membrane interlayer with Pt recombination particles for reduction of the anodic hydrogen content in PEM water electrolysis." Journal of The Electrochemical Society, vol. 165, no. 16, 2018, pp. F1271–F1277, https://doi.org/10.1149/2.1241814jes.

[47] Jung, A., Oh, J., Han, K., & Kim, M.S. (2016). An experimental study on the hydrogen crossover in polymer electrolyte membrane fuel cells for various current densities. Applied Energy, 175, 212–217. https://doi.org/10.1016/j.apenergy.2016.05.016.

[48] Suzuki, A., Sen, U., Hattori, T., Miura, R., Nagumo, R., Tsuboi, H., Hatakeyama, N., Endou, A., Takaba, H., Williams, M.C., & Miyamoto, A. (2011). Ionomer content in the catalyst layer of polymer electrolyte membrane fuel cell (PEMFC): effects on diffusion and performance. International Journal of Hydrogen Energy, 36(3), 2221–2229. https://doi.org/10.1016/j.ijhydene.2010.11.076.

[49] Reksten, A. H., Thomassen, M. S., Møller-Holst, S., & Sundseth, K. (2022). Projecting the future cost of PEM and alkaline water electrolyzers; a CAPEX model including electrolyzer plant size and technology development. International Journal of Hydrogen Energy, 47(90), 38106-38113. https://doi.org/10.1016/j.ijhydene.2022.08.306.

[50] IEA, Announced electrolyzer manufacturing capacity by region and manufacturing capacity needed in the Net Zero Scenario, 2021-2030, IEA, Paris https://www.iea.org/data-and-statistics/charts/announced-electrolyzer-manufacturing-capacity-by-region-and-manufacturing-capacity-needed-in-the-net-zero-scenario-2021-2030 , IEA. Licence: CC BY 4.0

[51] Spreitzer, Daniel, and Johannes Schenk. "Reduction of Iron Oxides with Hydrogen—A Review." *Steel Research International*, vol. 90, no. 10, 2019, p. 1900108, https://doi.org/10.1002/srin.201900108

[52] Fischedick, Manfred, et al. "Techno-economic Evaluation of Innovative Steel Production Technologies." *Journal of Cleaner Production*, vol. 84, 2014, pp. 563-580, https://doi.org/10.1016/j.jclepro.2014.05.063

[53] LeRoy, R. L., Bowen, C. T., & LeRoy, D. J. (1980). The Thermodynamics of Aqueous Water Electrolysis. Journal of The Electrochemical Society, 127(9), 1954. https://doi.org/10.1149/1.2130044

[54] Kopitzke, R. W., Linkous, C. A., Anderson, H. R., Nelson, G. L. (2000). Conductivity and Water Uptake of Aromatic-Based Proton Exchange Membrane Electrolytes. Journal of The Electrochemical Society, 147(5), 1677. https://doi.org/10.1149/1.1393417.

[55] Ito, H., Maeda, T., Nakano, A., & Takenaka, H. (2011). Properties of Nafion membranes under PEM water electrolysis conditions. International Journal of Hydrogen Energy, 36(17), 10527-10540. https://doi.org/10.1016/j.ijhydene.2011.05.127

[56] Ogumi, Z., Takehara, Z., & Yoshizawa, S. (1984). Gas Permeation in SPE Method: I. Oxygen Permeation Through Nafion and NEOSEPTA. Journal of The Electrochemical Society, 131(4), 769. https://doi.org/10.1149/1.2115696

[57] Mann, R. F., Amphlett, J. C., Peppley, B. A., & Thurgood, C. P. (2006). Henry's Law and the solubilities of reactant gases in the modeling of PEM fuel cells. Journal of Power Sources, 161(2), 768-774. https://doi.org/10.1016/j.jpowsour.2006.05.054.

[58] Bernardi, D. M., & Verbrugge, M. W. (1991). Mathematical model of a gas diffusion electrode bonded to a polymer electrolyte. AIChE Journal, 37, 1151-1163. https://api.semanticscholar.org/CorpusID:93166767

[59] Babic, U., Suermann, M., Büchi, F. N., Gubler, L., & Schmidt, T. J. (2017). Critical Review—Identifying Critical Gaps for Polymer Electrolyte Water Electrolysis Development. Journal of The Electrochemical Society, 164(4), F387. https://doi.org/10.1149/2.1441704jes

[60] Eurostat. (2021). Electricity price statistics, first half 2021. [cited 2021, December 13]. Available from: https://ec.europa.eu/eurostat/statistics-explained/index.php?title=Electricity_price_statistics

[61] Ulleberg, Ø., & Hancke, R. (2020). Techno-economic calculations of small-scale hydrogen supply systems for zero emission transport in Norway. International Journal of Hydrogen Energy, 45(2), 1201-1211. https://doi.org/10.1016/j.ijhydene.2019.05.170.

[62] FUEL CELLS and HYDROGEN 2 JOINT UNDERTAKING (FCH 2 JU). (2018). Addendum to the Multi-Annual Work Plan 2014-2020. Retrieved from http://fch.europa.eu/page/multi-annual-work-plan

[63] Springer, T. E., Zawodzinski, T. A., & Gottesfeld, S. (1991). Polymer Electrolyte Fuel Cell Model. Journal of The Electrochemical Society, 138(8), 2334. https://doi.org/10.1149/1.2085971.

[64] Onda, K., Murakami, T., Hikosaka, T., Kobayashi, M., Notu, R., & Ito, K. (2002). Performance Analysis of Polymer-Electrolyte Water Electrolysis Cell at a Small-Unit Test Cell and Performance Prediction of Large Stacked Cell. Journal of The Electrochemical Society, 149(8), A1069. https://doi.org/10.1149/1.1492287.

[65] GEP. (n.d.). Outlook for green and blue hydrogen market. GEP. https://www.gep.com/blog/strategy/Green-and-blue-hydrogen-current-levelized-cost-of-production-and-outlook#:~:text=The%20current%20levelized%20cost%20of,procurement%20cost%20of%20renewable%20electricity.